

1 Terrestrial ecosystem carbon flux estimated using GOSAT and OCO-2 XCO₂ re- 2 trievals

3 Hengmao Wang¹, Fei Jiang^{1,2*}, Jun Wang¹, Weimin Ju¹, Jing M. Chen^{1,3}

4 *1 Jiangsu Provincial Key Laboratory of Geographic Information Science and Technology, International Institute for*
5 *Earth System Science, Nanjing University, Nanjing, 210023, China*

6 *2 Jiangsu Center for Collaborative Innovation in Geographical Information Resource Development and Application,*
7 *Nanjing, 210023, China*

8 *3, Department of Geography, University of Toronto, Toronto, Ontario M5S3G3, Canada*

9

10 Abstract

11 In this study, both the Greenhouse Gases Observing Satellite (GOSAT) and the Orbiting Car-
12 bon Observatory 2 (OCO-2) XCO₂ retrievals produced by NASA Atmospheric CO₂ Observations
13 from Space (ACOS) project (Version b7.3), are assimilated within the GEOS-Chem 4D-Var assimi-
14 lation framework to constrain the terrestrial ecosystem carbon flux during Oct 1, 2014 to Dec 31,
15 2015. For the comparison, one inversion using in-situ CO₂ observations, and another for benchmark,
16 using global atmospheric CO₂ growth rate, are also conducted. The estimated global and regional
17 carbon fluxes for 2015 are shown and discussed. CO₂ observations from surface flask sites and XCO₂
18 retrievals from TCCON sites are used to evaluate the simulated concentrations with the posterior
19 carbon fluxes. The results show that globally, the terrestrial ecosystem carbon sink (excluding bio-
20 mass burning emissions) estimated from GOSAT data is stronger than that inferred from OCO-2 data,
21 and the annual atmospheric CO₂ growth rate estimated from GOSAT data is more consistent with the
22 benchmark inversion. Regionally, in most regions, the land sinks inferred from GOSAT data are also
23 stronger than those from OCO-2 data. Compared with the prior fluxes, the carbon fluxes in northern
24 temperate regions change the most, followed by tropical and southern temperate regions, and the
25 smallest changes occur in boreal regions. In temperate regions, the prior land sinks are significantly

* Corresponding author: Tel.: +86-25-83597077; Fax: +86-25-83592288; E-mail address: jiangf@nju.edu.cn

26 increased, while in tropical regions the prior land sinks are decreased. The different changes in dif-
27 ferent regions are mainly related to the spatial coverage and the data amount of XCO₂, and the devi-
28 ations between the retrieved and pre-modeled XCO₂ in these regions. The uncertainties of the two
29 retrievals may also have impact on their performances during the inversion. Evaluations using flask
30 and TCCON observations and the comparisons with in situ and benchmark inversions suggest that
31 GOSAT data, can effectively improve the carbon flux estimates in the northern hemisphere.

32 **Keywords:** Terrestrial ecosystem carbon flux, inversion, GOSAT, OCO-2, GEOS-Chem

33

34 1. Introduction

35 Atmospheric inverse modeling is an effective method for quantifying surface carbon fluxes at
36 global and regional scales using the gradient of CO₂ measurements. Inversion studies based on in-
37 situ CO₂ observations agree well on global carbon budget estimates but differ greatly on regional
38 carbon flux estimates and the partitioning of land and ocean fluxes as well, mainly due to the sparse-
39 ness of observations in tropics, southern hemisphere oceans and the majority of continental interiors
40 such as those in South America, Africa, and Boreal Asia (Peylin et al., 2013). Satellite observations
41 offer an attractive means to constrain atmospheric inversions with their extensive spatial coverage
42 over remote regions. Studies have shown that, theoretically, satellite observations, though with lower
43 precision than in-situ measurements, can improve the carbon flux estimates (Rayner and O'Brien,
44 2001; Pak and Prather, 2001; Houweling et al., 2004; Baker et al., 2006; Chevallier et al., 2007; Miller
45 et al., 2007; Kadyrov et al., 2009; Hungershofer et al., 2010).

46 Satellite sensors designed specifically to retrieve atmospheric CO₂ concentrations, have been in
47 operation in recent years. The Greenhouse Gases Observing Satellite (GOSAT) (Kuze et al., 2009),
48 being the first satellite mission dedicated to observing CO₂ from space, was launched in 2009. The
49 National Aeronautics and Space Administration (NASA) launched the Orbiting Carbon Observa-

50 tory 2 (OCO-2) satellite in 2014 (Crisp et al., 2017; Eldering et al., 2017). China's first CO₂ moni-
51 toring satellite (TanSat) was launched in 2016 (Wang et al., 2017; Yang et al., 2017). These satel-
52 lites measure near-infrared sunlight reflected from the surface in CO₂ spectral bands and the O₂ A-
53 band to retrieve column-averaged dry-air mole fractions of CO₂ (XCO₂), aiming to improving the
54 estimation of spatial and temporal distributions of carbon sinks and sources. A number of inversions
55 have utilized GOSAT XCO₂ retrievals to infer surface carbon fluxes (Basu et al., 2013; Maksyutov
56 et al., 2013; Saeki et al., 2013; Chevallier et al., 2014; Deng et al., 2014; Houweling et al., 2015;
57 Deng et al, 2016). Although large uncertainty reductions were achieved for regions which are un-
58 der-sampled by in-situ observations, these studies didn't give robust regional carbon flux estimates.
59 There are large spreads in regional flux estimates in some regions among these inversions. Further-
60 more, regional flux distributions inferred from GOSAT XCO₂ data are significantly different from
61 those inferred from in-situ observations. For instance, several studies using GOSAT retrievals re-
62 ported a larger than expected carbon sink in Europe (Basu et al., 2013; Chevallier et al., 2014; Deng
63 et al., 2014; Houweling et al., 2015). The validity of this large Europe carbon sink derived from
64 GOSAT retrievals is in intense debate and efforts to improve the accuracy of Europe carbon sink
65 estimate are still ongoing (Reuter et al., 2014; Feng et al., 2016; Reuter et al., 2017).

66 Compared with GOSAT, OCO-2 has a higher sensitivity to column CO₂, much finer footprints
67 and more extended spatial coverage, and thus has the potential to better constrain the surface carbon
68 flux inversion (Eldering et al., 2017). Studies have used OCO-2 XCO₂ data to estimate carbon flux
69 anomalies during recent El Nino events (Chatterjee et al., 2017; Patra et al., 2017; Heymann et al.,
70 2017; Liu et al., 2017). Nassar et al. (2017) applied OCO-2 XCO₂ data to infer emissions from large
71 power plants. Miller et al. (2018) evaluated the potential of OCO-2 XCO₂ data in constraining re-
72 gional biospheric CO₂ fluxes and found that in the current state of development, OCO-2 observa-
73 tions can only provide a reliable constraint on CO₂ budget at continental and hemispheric scales. At

74 present, it is still not clear whether with the improved monitoring capabilities, current OCO-2 ob-
75 servations have a greater potential than GOSAT observations for estimating CO₂ flux at regional or
76 finer scale. It is therefore important to investigate how current OCO-2 XCO₂ data differ from GO-
77 SAT XCO₂ data in constraining carbon budget.

78 In this study, we evaluate the performance of GOSAT and OCO-2 XCO₂ data in constraining
79 terrestrial ecosystem carbon flux. GOSAT and OCO-2 XCO₂ retrievals produced by the NASA At-
80 mospheric CO₂ Observations from Space (ACOS) team are applied to infer monthly terrestrial eco-
81 system carbon sinks and sources from Oct, 2014 through December, 2015, using a 4D-Var scheme
82 based on the GEOS-Chem Adjoint model (Henze et al., 2007). To evaluate the performance of satel-
83 lite XCO₂ data based inversions, we conduct two additional inversions using in situ measurements
84 and the global CO₂ trend, respectively. For simplicity, four inversions are referred as OCO-2 inver-
85 sion, GOSAT inversion, in situ inversion and benchmark inversion, respectively. Inversion results are
86 also evaluated against surface flask CO₂ observations and Total Carbon Column Observing Network
87 (TCCON) XCO₂ retrievals. This paper is organized as follows. Section 2 briefly introduces GOSAT
88 and OCO-2 XCO₂ retrievals and the inversion methodology and settings. Results and discussions are
89 presented in Section 3, and Conclusions are given in Section 4.

90

91 **2. Data and Method**

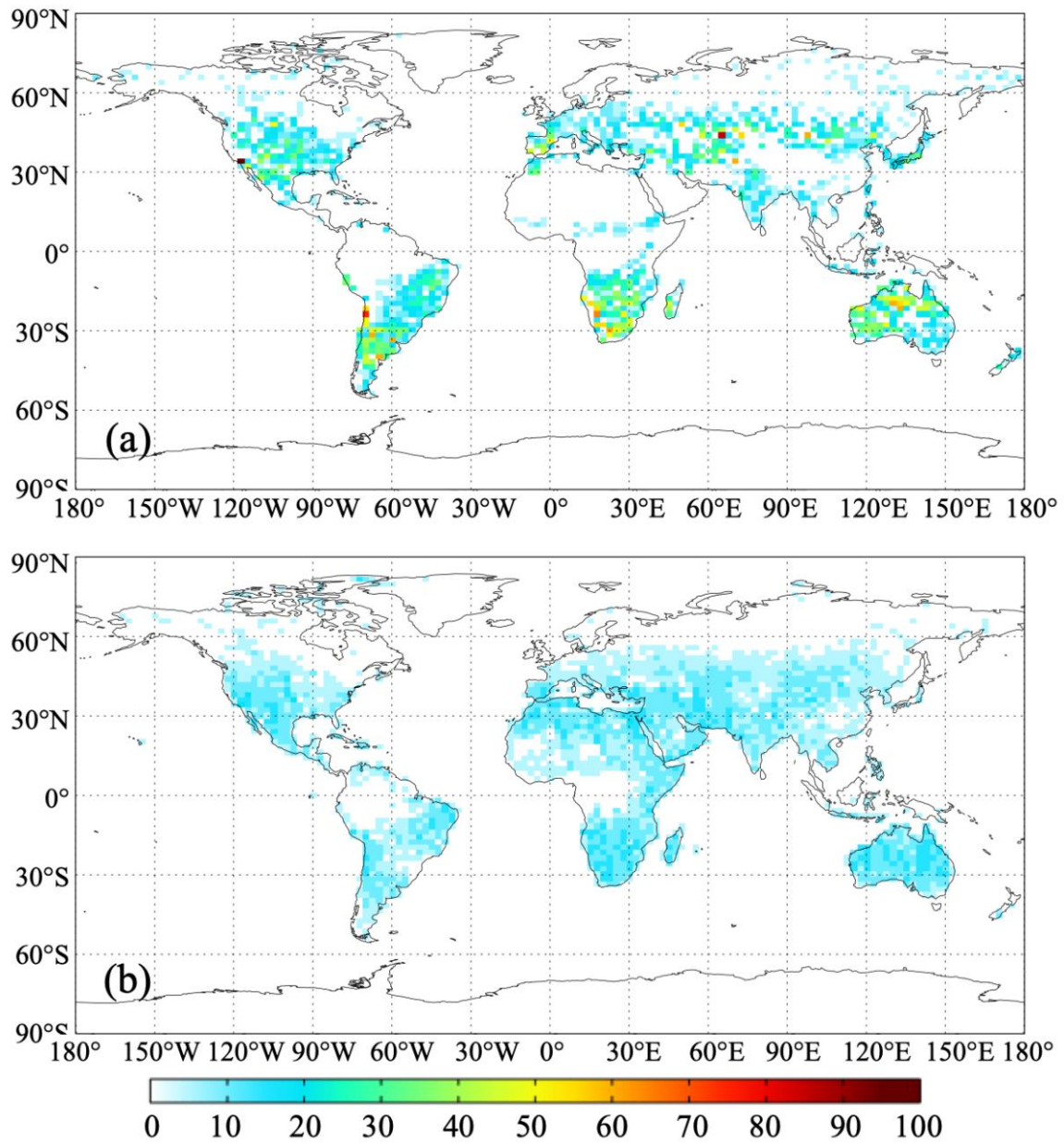
92 2.1 GOSAT and OCO-2 XCO₂ retrievals

93 Developed jointly by the National Institute for Environmental Studies (NIES), the Japanese
94 Space Agency (JAXA) and the Ministry of the Environment (MOE) of Japan, GOSAT was de-
95 signed to retrieve total column abundances of CO₂ and CH₄. The satellite flies at a 666 km altitude
96 in a sun-synchronous orbit with 98° inclination that crosses the equator at 12:49 local time. It co-
97 vers the whole globe in three days and has a footprint of 10.5 km² at nadir. OCO-2 is NASA's first
98 mission dedicated to retrieving atmospheric CO₂ concentration. It flies at 705 km altitude in a sun-

99 synchronous orbit with an overpass time at approximately 13:30 local time and a repeat cycle of 16
100 days. Its grating spectrometer measures reflected sunlight in three near-infrared regions (0.765, 1.61
101 and 2.06 μm) to retrieve XCO₂. OCO-2 has a footprint of 1.29×2.25 km² at nadir and acquires eight
102 cross-track footprints creating a swath width of 10.3 km.

103 Both GOSAT and OCO-2 XCO₂ products were created using the same retrieval algorithm,
104 which is based on a Bayesian optimal estimation approach (Roggers et al., 2000; O Dell et al.,
105 2011). The GOSAT and OCO-2 XCO₂ data used in this study are Version 7.3 Level 2 Lite products
106 at the pixel level. The XCO₂ data from lite products are bias-corrected (Wunch et al., 2011). Before
107 being used in our inversion system, the data are processed in three steps. First, the retrievals for the
108 glint soundings over oceans have relatively larger uncertainty, thus the data over oceans are not
109 used in our inversions (Wunch et al., 2017). Second, in order to achieve the most extensive spatial
110 coverage with the assurance of using best quality data available, the XCO₂ data are filtered with two
111 parameters, namely warn_levels and xco2_quality_flag, which are provided along with the XCO₂
112 data. All data with xco2_quality_flag not equaling 0 are removed, the rest are divided into three
113 groups according the value of warn_levels, namely group 1, group 2 and group 3. In group 1, the
114 warn_levels are less than 8, in group 2, the warn_levels are greater than 9 and less than 12, and in
115 group 3, those are greater than 13. Group 1 has the best data quality, followed by group 2, and
116 group 3 is the worst. Third, the pixel data are averaged within the grid cell of 2°×2.5°, which is the
117 resolution of the global atmospheric transport model used in this study. In each grid of 2°×2.5°,
118 only the groups of best data quality are selected and then averaged. The other variables like column
119 averaging kernel, retrieval error and so on which are provided along with the XCO₂ product are also
120 dealt with the same method. Figures 1a and 1b show the coverages and data amount of GOSAT
121 and OCO-2 XCO₂ data during the study period after processing. The filtered GOSAT and OCO-2
122 retrievals are not evenly distributed spatially. Due to the cloud contamination, there are few retriev-
123 als in a large portion of tropical land. In northern high latitude area, especially in boreal regions,

124 due to the low solar zenith angle, available satellite retrievals are very sparse.



125

126 **Figure 1.** Data amount of each grid cell (2°x2.5°) of ACOS XCO₂ used in this study (a, GOSAT; b,
127 OCO-2)

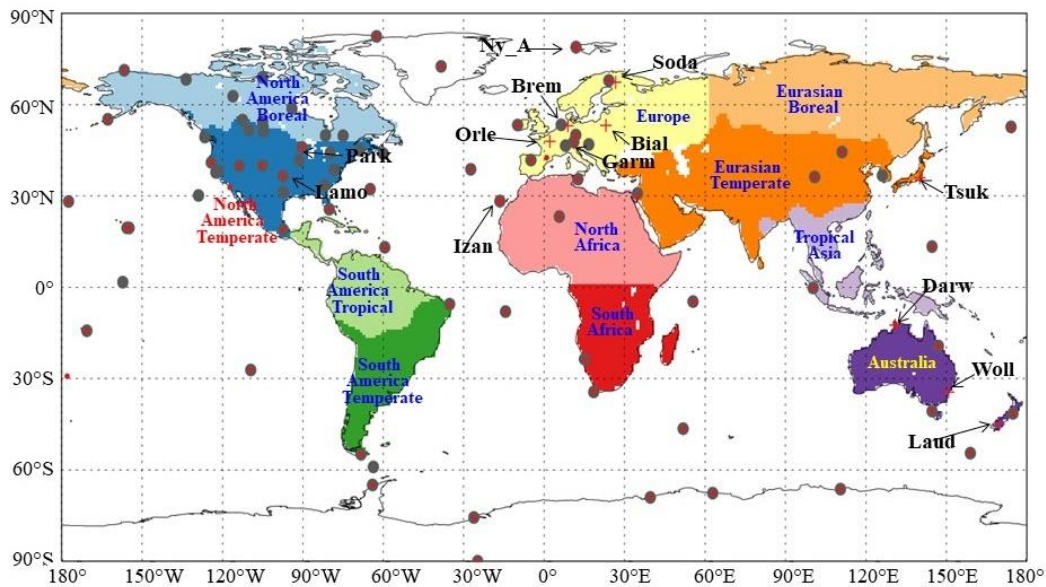
128 2.2 Surface observations and TCCON XCO₂ retrievals

129 Surface CO₂ observations are from the obspack_co2_1_CARBONTRACKER_CT2016_2017-

130 02-06 product (ObsPackCT2016) (CarbonTracker Team, 2017), which was the observation data

131 used in CarbonTracker 2016 (Peters et al., 2007, with updates documented at <http://carbon-tracker.noaa.gov>). It is a subset of the Observation Package (ObsPack) Data Product (ObsPack, 132 2016), and contains a collection of discrete and quasi-continuous measurements at surface, tower 133 and ship sites contributed by national and universities laboratories around the world. In this study, 134 In situ measurements from 78 sites provided by this product are used for inversion. Among these 78 135 sites, there are 56 flask sites, of which 52 sites are selected to evaluate the posterior CO₂ concentra- 136 tions (selection criteria given in Section 4.3.1). 137

138 TCCON is a network of ground-based Fourier Transform Spectrometers that measure direct 139 near-infrared solar absorption spectra. Column-averaged abundances of atmospheric constituents 140 including CO₂, CH₄, N₂O, HF, CO, H₂O, and HDO are retrieved through these spectra. We use 141 XCO₂ retrievals from 13 stations from TCCON GGG2014 dataset (Blumenstock et al., 2017; 142 Deutscher et al., 2017; Griffith et al., 2017a, b; Kivi et al., 2017; Morino et al., 2017; Notholt et al., 143 2017a, b; Sherlock et al., 2017; Sussmann and Rettinger, 2017; Warneke et al., 2017; Wennberg et 144 al., 2017a, b). The locations of in situ sites and 13 TCCON stations are shown in Figure 2.



145 **Figure 2.** Distributions of the observation sites used in this study. Gray solid circles are surface 146 sites used in the in situ inversion, red points and red cross marks are surface flask and TCCON sites 147 used for evaluations, respectively, the shaded shows the 11 TRANSCOM regions 148

149 **2.3 GEOS-Chem 4DVAR assimilation framework**

150 **2.3.1 GEOS-Chem model**

151 GEOS-Chem model (<http://geos-chem.org>) is a global three-dimensional chemistry transport
152 model (CTM), which is driven by assimilated meteorological data from the Goddard Earth Observ-
153 ing System (GEOS) of the NASA Global Modeling and Assimilation Office (GMAO) (Rienecker et
154 al., 2008). The original CO₂ simulation in the GEOS-Chem model was developed by Suntharalin-
155 gam et al. (2004) and accounts for CO₂ fluxes from fossil fuel combustion and cement production,
156 biomass burning, terrestrial ecosystem exchange, ocean exchange and biofuel burning. Nassar et al.
157 (2010) updated the CO₂ simulation with improved inventories. In addition to the inventories in ear-
158 lier version, the new CO₂ fluxes includes CO₂ emissions from international shipping, aviation (3D)
159 and the chemical production of CO₂ from CO oxidation throughout the troposphere. In most other
160 models, the oxidation of CO was treated as direct surface CO₂ emissions. The details of the CO₂
161 simulation and the CO₂ sinks/sources inventories could be found in Nassar et al. (2010). The ver-
162 sion of GEOS-Chem model used in this study is v8-02-01.

163 **2.3.2 GEOS-Chem adjoint model**

164 An adjoint model is used to calculate the gradient of a response function of one model scalar
165 (or cost function) with respect to a set of model parameters. The adjoint of the GEOS-Chem model
166 was first developed for inverse modeling of aerosol (or their precursors) and gas emissions (Henze
167 et al., 2007). It has been implemented to constrain sources of species such as CO, CH₄, and O₃ with
168 satellite observations (Kopacz et al., 2009, 2010; Jiang et al., 2011; Wecht et al., 2012; Parrington et
169 al., 2012). Several studies have successfully used this adjoint model to constraint carbon sources
170 and sinks with surface flask measurements of CO₂ mixing ratio and space-based XCO₂ retrievals
171 (Deng et al., 2014; Liu et al., 2014; Deng et al., 2016; Liu et al., 2017).

172 **2.3.3 Inversion method**

173 In the GEOS-Chem inverse modeling framework, the 4D-Var data assimilation technique is

174 employed for combining observations and simulations to seek a best optimal estimation of the state
 175 of a system. The scaling factors are applied to the carbon flux components to be optimized monthly
 176 in each model grid point. This approach seeks the scaling factors of the carbon flux that minimize
 177 the cost function, J , given by:

$$178 \quad J(c) = \frac{1}{2} \sum_{i=1}^N (XCO_{2,i}^m - XCO_{2,i}^{obs}) S_{obs,i}^{-1} (XCO_{2,i}^m - XCO_{2,i}^{obs}) + \left(\frac{1}{2} (c - c_a) S_c^{-1} (c - c_a) \right)$$

179 where N is total number of satellite XCO_2 observations; XCO_2^m and XCO_2^{obs} are modeled and ob-
 180 served total column averaged dry air mole fraction of CO_2 respectively; c_a is the prior scaling factor
 181 of the carbon flux, which is typically set as unity; S_{obs} is the model-data mismatch error covariance
 182 matrix; S_c is the scaling factor error covariance matrix. The gradients of the cost function with re-
 183 spect to scaling factors calculated with the adjoint model are supplied to an optimization routine
 184 (the L-BFGS-B optimization routine; Byrd et al., 1995; Zhu et al., 1994), and the minimum of the
 185 cost function is sought iteratively.

186 For the modeled CO_2 column to be comparable with the satellite XCO_2 retrievals, the modeled
 187 CO_2 concentration profile should be first mapped into the satellite retrieval levels and then convo-
 188 luted with retrieval averaging kernels. The modeled XCO_2 is computed by:

$$189 \quad XCO_2^m = XCO_2^a + \sum_j h_j a_j (A(x) - y_{a,j})$$

190 where j denotes retrieval level, x is the modeled CO_2 profile; $A(x)$ is a mapping matrix; XCO_2^a is prior
 191 XCO_2 , h_j is pressure weighting function, a_j is the satellite column averaging kernel and y_a is the prior
 192 CO_2 profile for retrieval. These last four quantities are provided from ACOS Version 7.3 Level 2 Lite
 193 products.

194 **3. Inversion settings**

195 In this study, the GEOS-Chem model was run in a horizontal resolution of $2^\circ \times 2.5^\circ$ for 47 verti-
196 cal layers. Four inversions, using GOSAT data, OCO-2 data, in-situ measurements and global at-
197 mospheric CO₂ trend are conducted from Oct 1, 2014 to December 31, 2015, respectively. The pos-
198 terior dry air mole fraction of CO₂ on Oct 1, 2014 from CT2016 product is taken as the initial con-
199 centration. The first three months are taken as the spin-up period. The prior carbon fluxes used in
200 this study include fossil fuel CO₂ emissions, biomass burning CO₂ emissions, terrestrial ecosystem
201 carbon exchange and CO₂ flux exchange over the sea surface. Fossil fuel emissions are obtained
202 from CT2016, which is an average of Carbon Dioxide Information Analysis Center (CDIAC) prod-
203 uct (Andres et al., 2011) and Open-source Data Inventory of Anthropogenic CO₂ (ODIAC) emis-
204 sion product (Oda and Maksyutov, 2011). The biomass burning CO₂ emissions are also taken from
205 CT2016, which are the average of the Global Fire Emissions Database version 4.1 (GFEDv4) (van
206 der Werf et al., 2010; Giglio et al., 2013) and the Global Fire Emission Database from NASA Car-
207 bon Monitoring System (GFED_CMS). The 3-hourly terrestrial ecosystem carbon exchanges are
208 from the Carnegie-Ames-Stanford Approach (CASA) model GFED4.1 simulation (Potter et al.,
209 1993; van der Werf et al., 2010). CO₂ exchanges over the ocean surface are from the posterior air-
210 sea CO₂ flux of CT2016. It is noted that the fossil fuel emissions and the biomass burning emissions
211 in our inversions are kept intact. Both terrestrial ecosystem CO₂ exchanges and ocean flux are opti-
212 mized in our inversions.

213 An efficient computational procedure for constructing non-diagonal scaling factor error covari-
214 ance matrix which accounts for the spatial correlation of errors is implemented (Single et al., 2011).
215 The construction is based on the assumption of exponential decay of error correlations. Other than
216 forming covariance matrix explicitly, multiple-dimensional correlations are represented by tensor
217 products of one-dimensional correlation matrices along longitude and latitudinal directions. For the
218 two inversions, the scale lengths assigned along longitudinal and latitudinal directions are 500 km

219 and 400 km for terrestrial ecosystem exchange and 1000 km and 800 km for ocean exchange, re-
220 spectively. No correlations between different types of fluxes are assumed. The temporal correla-
221 tions are also neglected. Global annual uncertainty of 100% and 40% are assigned for terrestrial
222 ecosystem and ocean CO₂ exchanges, respectively (Deng and Chen, 2011). Accordingly, the uncer-
223 tainty of scaling factor for the prior land and ocean fluxes in each month at the grid cell level are
224 assigned to 3 and 5, respectively.

225 3.1 Inversions using satellite XCO₂ retrievals

226 The observation error covariance matrix is constructed using the retrieval errors, which are pro-
227 vided along with the ACOS XCO₂ data. Observation errors are assumed to be uncorrelated at model
228 grid level. To account for the correlated observation errors, as shown in section 2.1, the pixel level
229 retrieval errors are filtered and averaged to the model grid level, and then inflated by a factor of 1.9
230 to ensure the chi-square testing of χ^2 value to be close to 1 (Tarantola, 2004; Chevallier et al.,
231 2007).

232 3.2 Inversion using in situ measurements

233 As described in section 2.2, surface CO₂ observations from 78 sites including flask samples
234 and by quasi-continuous analyzer are adopted in this inversion. These data are selected from data
235 collection of the ObsPackCT2016. The observation uncertainties of the 78 sites are also obtained
236 from this product, which account for both the measurement and representative errors (Peters et al.,
237 2007, with updates documented at <http://carbontracker.noaa.gov>). An examination for the differ-
238 ences between observations and forward model simulation was conducted (data not shown), and the
239 results shows that observation uncertainties from CT2016 represents well with the model-data mis-
240 match errors of GEOS-Chem model. In addition, we neglect correlations between observations and
241 assume a diagonal observation error covariance matrix.

242 3.3 Benchmark inversion

243 A baseline inversion, which was introduced by Chevalier et al.(2009) as a Poor Man's method,

244 is implemented to evaluate satellite retrievals and in situ measurements based inversions. Usually,
245 the posteriori fluxes are evaluated by the improvement on the simulated CO₂ mixing ratios. Since
246 the global CO₂ trend can be accurately estimated from marine sites, it is important to assess whether
247 the inverted flux can capture more information than this trend. In this baseline inversion, the ocean
248 flux is kept identical to the prior ones. The poor man's inverted land flux F_{pm} at location (x, y) and
249 at time t is defined as:

$$250 \quad F_{pm}(x, y, t) = F_{prior}(x, y, t) + k \times \sigma(x, y, t)$$

251 where F_{prior} is the prior flux, σ is the uncertainty of the prior flux, k is a coefficient. Here k is de-
252 termined by trial and error so that the mean annual global total of the poor man's fluxes equals the
253 mean global total given by the annual global CO₂ growth rate from the Global Monitoring Division
254 (GMD) of NOAA/Earth System Research Laboratory (ESRL) (Ed Dlugokencky and Pieter Tans,
255 NOAA/ESRL, www.esrl.noaa.gov/gmd/ccgg/trends/). The annual global CO₂ growth rate is 2.96
256 ppm in 2015, which is converted to 6.28 PgC yr⁻¹ for the poor man's global total by multiply by a
257 factor of 2.123 PgC ppm⁻¹. In practice, this method distributes the land carbon sink according to the
258 gross carbon fluxes from the vegetation.

259 **4. Results and Discussions**

260 **4.1 Global carbon budget**

261 Table 1 presents the inverted global carbon budgets in 2015 from four inversions. The global
262 land sinks inferred by GOSAT and OCO-2 XCO₂ retrievals are -3.48 and -2.94 PgC yr⁻¹, respec-
263 tively, which are both larger than the prior value, and lower than the estimate from the in-situ inver-
264 sion. The global net flux from the benchmark inversion is inferred from the global annual CO₂
265 growth rate, which represents relatively accurately the net carbon flux added into atmosphere. It
266 could be found that the global net flux from GOSAT inversion is the closest to the benchmark inver-
267 sion estimate, while the one from OCO-2 inversion is higher and the in situ inversion estimate is

268 lower than the benchmark estimate. The differences of ocean fluxes among a priori and two inver-
 269 sions are small since we don't assimilate XCO₂ data over ocean. Therefore, the differences for the
 270 global net fluxes among the different experiments are similar to those of the global land sinks, indi-
 271 cating that GOSAT experiment has the best estimates for the land and ocean carbon uptakes, while
 272 those from in situ inversion are overestimated, and from OCO-2 inversion might be underestimated.

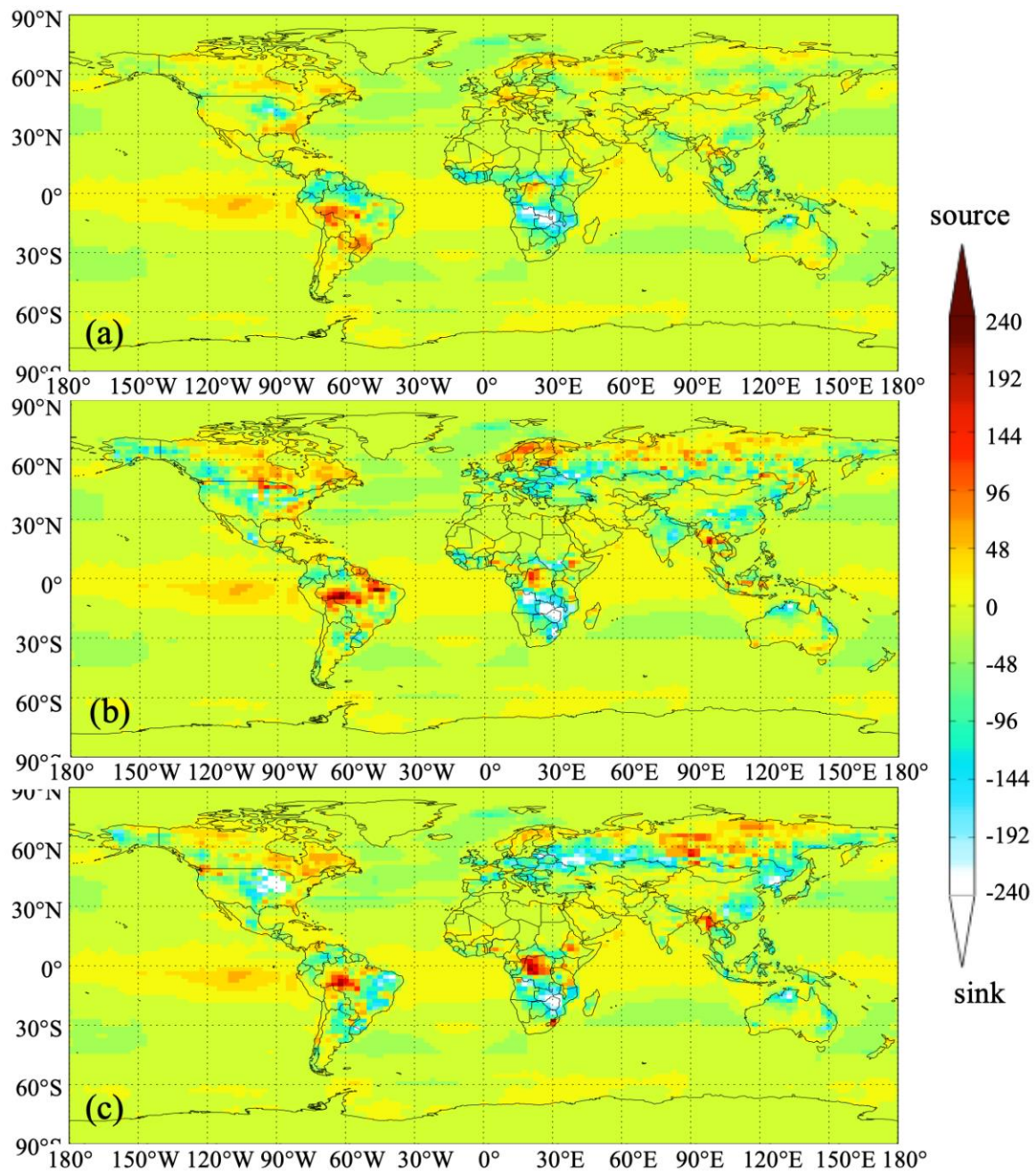
273 **Table 1.** Global carbon budgets estimated by the OCO-2 and GOSAT inversions in this study as well
 274 as those from the prior fluxes, In situ and benchmark inversions (PgC yr⁻¹)

	Prior	OCO-2	GOSAT	In situ	Benchmark
Fossil fuel and industry	9.84	9.84	9.84	9.84	9.84
Biomass burning emissions	2.2	2.2	2.2	2.2	2.2
Land sink	-2.5	-2.94	-3.48	-3.63	-3.35
Ocean sink	-2.41	-2.44	-2.45	-2.41	-2.41
Global net flux	7.13	6.66	6.11	6.0	6.28

275

276 4.2 Regional carbon flux

277 Figure 3 shows the distributions of annual land and ocean carbon fluxes (excluding fossil fuel
 278 and biomass burning carbon emissions, same thereafter) of the prior and the estimates using GOSAT
 279 and OCO-2 data. It could be found that compared with the prior fluxes, the carbon sinks in Central
 280 America, south and northeast China, east and central Europe, south Russia and east Brazil are obvi-
 281 ously increased in GOSAT inversion. Except for east Brazil, the land sinks in those areas in OCO-2
 282 inversion are also increased, but much weaker than those in GOSAT inversion, and in east Brazil, it
 283 turns to a significant carbon source. In contrast, in east and central Canada, north Russia, north Eu-
 284 rope, west Indo-China Peninsula, north Democratic Republic of the Congo and west Brazil, their
 285 carbon sources are significantly increased in both GOSAT and OCO-2 inversions. In east and central
 286 Canada, north Europe and west Brazil, there are much stronger carbon sources in OCO-2 inversion.



287

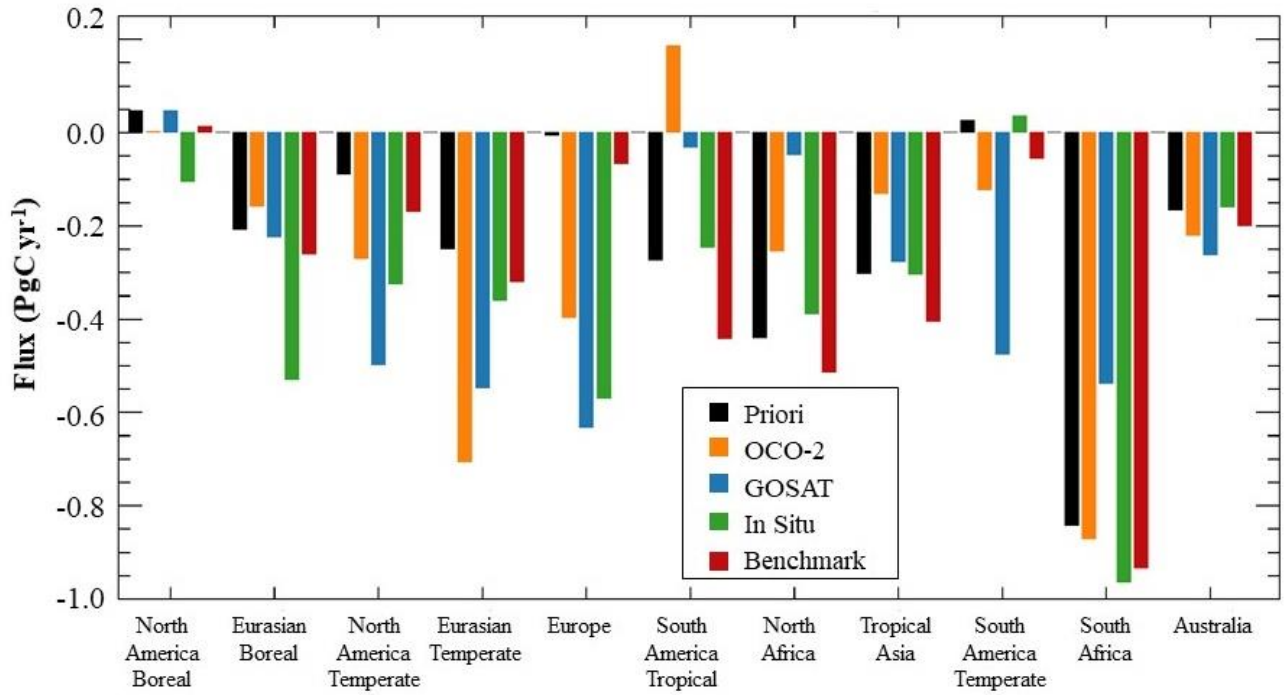
288 **Figure 3.** Distributions of annual land and ocean carbon fluxes a) prior flux and posterior fluxes
 289 based on (b) OCO-2 and (c) GOSAT data ($\text{gC m}^{-2}\text{yr}^{-1}$)
 290

291

292 To better investigate the differences between GOSAT and OCO-2 inversions as well as their
 293 differences with the prior fluxes and two other inversions, we aggregate the prior and inferred land
 294 fluxes into 11 TRANSCOM land regions (Gurney et al., 2002) as shown in Figure 2. Figure 4 shows
 295 aggregated annual land surface fluxes from the prior and four inversions for the 11 land regions.
 Clearly, in most regions, the land sinks inverted based on GOSAT data are stronger than those inferred

296 from OCO-2 data, especially in the Temperate and Tropical Lands. For example, in South America
297 Temperate, the estimated land sink based on GOSAT data is about 4 times as large as the OCO-2
298 inversions; in North America Temperate and Tropical Asia, the carbon sinks of GOSAT experiment
299 is about twice that of the OCO-2 inversions; and in South America Tropical, the OCO-2 inversion
300 result is a carbon source of 0.19 PgC yr^{-1} , while GOSAT inversion gives a weak sink of -0.05 Pg C
301 yr^{-1} . The total sinks of the Temperate/Tropical Lands optimized using GOSAT and OCO-2 XCO_2
302 retrievals are $-2.95/-0.36$ and $-2.59/-0.20 \text{ Pg C yr}^{-1}$, respectively (Table 2). In Northern Boreal Land,
303 the total carbon sinks inverted with GOSAT and OCO-2 data are comparable. However, the two XCO_2
304 data have opposite performances in these two areas, namely in Eurasian Boreal, the inverted land sink
305 with GOSAT is stronger than that with OCO-2; while in North America Boreal, it is the opposite.

306 For different continents (Table 2), in Asia and Australia, their carbon sinks inverted from GOSAT
307 and OCO-2 data are comparable. In North America, South America and Europe, the land sinks in
308 GOSAT inversion are much stronger than those in OCO-2 inversion. Especially in South America,
309 the GOSAT inversion result is a strong carbon sink ($-0.51 \text{ Pg C yr}^{-1}$), while in OCO-2 inversion, it is
310 a weak carbon source ($0.06 \text{ Pg C yr}^{-1}$). Conversely, in Africa, the land sink estimated with GOSAT
311 data is much weaker than those from OCO-2 data, the former ($-0.59 \text{ Pg C yr}^{-1}$) being only about the
312 half of the latter ($-1.13 \text{ Pg C yr}^{-1}$).



313

314

Figure 4. Aggregated annual land fluxes of the 11 TRANSCOM land regions

315

316

Table 2. The prior and posterior fluxes in six continents and boreal, temperate and tropical lands

Regions	Prior	OCO-2	GOSAT	In situ	Benchmark
North America	-0.04	-0.27	-0.45	-0.42	-0.15
South America	-0.25	0.06	-0.51	-0.04	-0.5
Europe	-0.01	-0.40	-0.63	-0.66	-0.07
Asia	-0.76	-0.99	-1.05	-1.16	-0.98
Africa	-1.28	-1.13	-0.58	-1.22	-1.45
Australia	-0.17	-0.22	-0.26	-0.13	-0.2
Northern Boreal Land	-0.16	-0.16	-0.18	-0.81	-0.25
Northern Temperate Land	-0.35	-1.37	-1.68	-1.22	-0.55
Tropical Land	-1.01	-0.20	-0.36	-0.49	-1.36
Southern Temperate Land	-0.98	-1.21	-1.28	-1.11	-1.2

317

318

319

Compared with the in situ and benchmark inversions, in the Boreal regions, the land sinks esti-

320

imated using in situ observations are much stronger than those of OCO-2 and GOSAT inversions, but

321 close to the benchmark results; in the Temperate lands, except for South Africa, the GOSAT results
322 are much stronger than those of the in situ and benchmark experiments, especially in South America
323 Temperate, GOSAT inversion shows a strong carbon sink, while in situ experiment shows a weak
324 source and benchmark experiment shows a weak sink; on the contrary, in the Tropical regions, the
325 land sinks inferred from both OCO-2 and GOSAT experiments are weaker than the in situ and bench-
326 mark inversions.

327 Compared with the prior fluxes, the inferred land fluxes in Northern Temperate regions have
328 the largest changes, followed by those in Tropical regions and Southern Temperate lands, while in
329 boreal regions, the changes are the smallest. As shown in Table 3, for different TRANSCOM regions
330 and different XCO₂ used, the changes of carbon fluxes have large differences. Since the same setup
331 used in these two inversions and the same algorithm adopted for retrieving XCO₂ from GOSAT and
332 OCO-2 measurements, the different impacts of XCO₂ data on land sinks may be related to the spatial
333 coverage and the amount of data in these two XCO₂ datasets. As shown in Figure 1, in different
334 latitude zones, the spatial coverage and the data amount of GOSAT and OCO-2 have large differences.
335 Statistics show that the amount of data is largest in northern temperate land, followed by southern
336 temperate land and tropical land, and least in northern boreal regions, corresponding to the magnitude
337 of changes of carbon fluxes in these zones. For one specific zone, the different impacts of these two
338 XCO₂ datasets may be also related to their data amount. For example, in northern temperate land,
339 GOSAT has more XCO₂ data than OCO-2. Accordingly, the change of carbon flux caused by GOSAT
340 is larger than that caused by OCO-2. Conversely, in Tropical Land, OCO-2 has more data than GO-
341 SAT, and as shown before it has more significant impact on the land sink. This relationship could also
342 be found in each TRANSCOM region. Figure 5 gives a relationship between the XCO₂ data amount
343 ratios of GOSAT to OCO-2 and the land sinks absolute change ratios caused by GOSAT to OCO-2
344 for 11 TRANSCOM land regions. Obviously, except for North and South Africa, there is a significant
345 linear correlation ($R=0.95$) between these two ratios, suggesting that with more XCO₂ data, the more

346 carbon flux relative to the prior flux is changed. In North Africa, we find that OCO-2 has better spatial
 347 coverage and more data than GOSAT, as shown in Figure 1. Although the differences mainly occur
 348 in the Sahara where the carbon flux is very weak, but near the equatorial region where the carbon
 349 flux is large, OCO-2 still has more data than GOSAT. In southern Africa, both XCO₂ have good
 350 spatial coverage, the amount of GOSAT data is about 1.5 times that of OCO-2, but the changes in the
 351 carbon flux caused by GOSAT is about 10 times that of OCO-2. The large ratio of carbon change is
 352 mainly due to the relatively small carbon change from OCO-2 inversion.

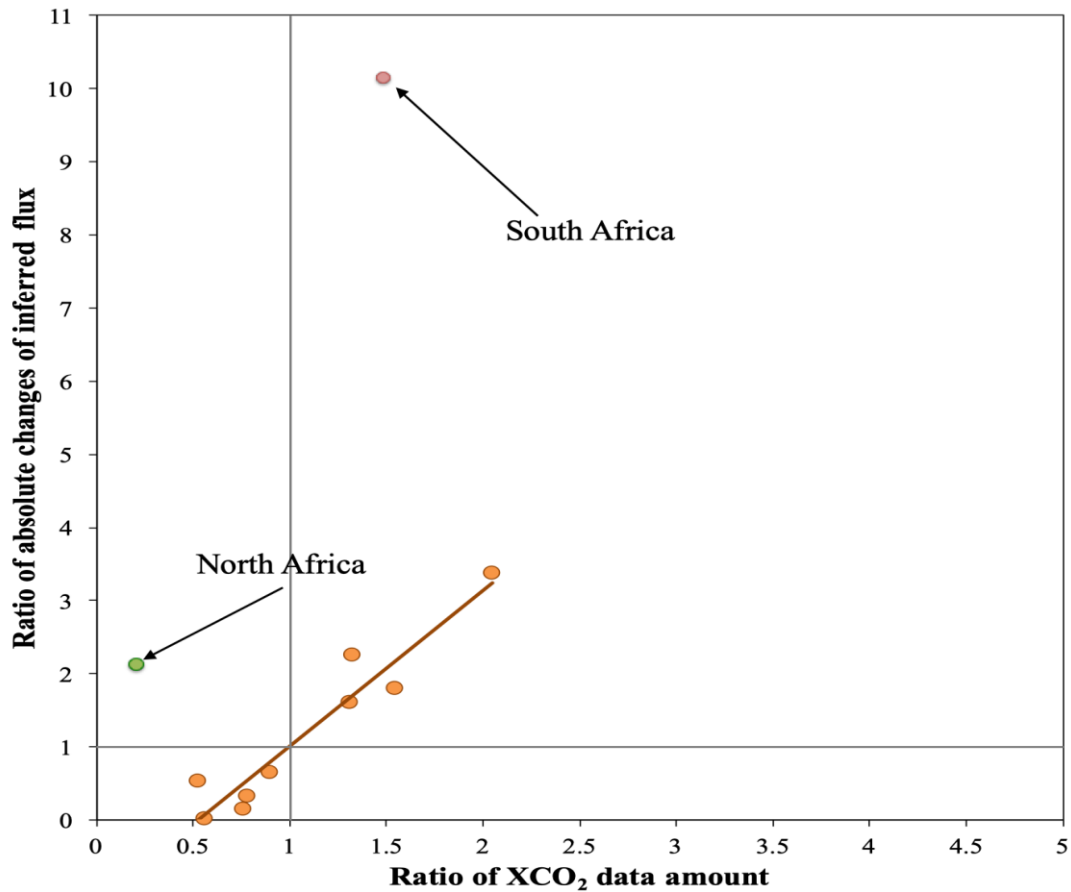
353

354 **Table 3.** Differences between the inferred and the prior carbon fluxes, the data amount of XCO₂ and
 355 the deviations between the modeled with prior flux and satellite retrieved XCO₂ in different regions

Region	Flux changed (Pg C yr ⁻¹)*		XCO ₂ data amount		Deviations (ppm)**	
	OCO-2	GOSAT	OCO-2	GOSAT	OCO-2	GOSAT
North America Boreal	-0.05	0	1143	639	0.6	1.41
North America Temperate	-0.18	-0.41	2390	3163	0.52	0.93
South America Tropical	0.46	0.24	800	421	-0.89	0.43
South America Temperate	-0.15	-0.5	1711	3500	0.02	0.54
North Africa	0.19	0.39	3208	674	0.12	-0.19
South Africa	-0.03	0.3	2057	3060	0.17	0.33
Eurasian Boreal	0.05	-0.02	1714	1339	0.47	1.5
Eurasian Temperate	-0.46	-0.3	5323	4782	0.46	0.82
Tropical Asia	0.17	0.03	726	550	-0.43	0.34
Australia	-0.05	-0.1	2011	3110	0.18	0.67
Europe	-0.39	-0.63	1604	2106	0.28	1.35
Global land	-0.44	-0.98	22687	23344	0.22	0.79
Northern Boreal Land	0.005	-0.02	2857	1978	0.52	1.47
Northern Temperate Land	-1.03	-1.33	9317	10051	0.45	0.96
Tropical Land	0.82	0.66	4734	1645	-0.08	0.13
Southern Temperate Land	-0.23	-0.3	5779	9670	0.11	0.6

356 * Differences between posterior and prior flux

357 ** Deviations between the modeled with prior flux and satellite retrieved XCO₂



358

359 **Figure 5.** Scatter plot for the ratio of GOSAT to OCO-2 XCO₂ data amount versus the ratio of abso-
 360 lute changes of the land sinks caused by GOSAT to OCO-2 in the 11 TRANSCOM land regions
 361

362 In addition to the data amount, the deviations between the simulated CO₂ concentrations using
 363 prior fluxes and the satellite retrievals should be another reason to explain the performances of
 364 OCO-2 and GOSAT retrievals in different regions. Usually, a large model-data mismatch will im-
 365 pose strong constraint on the prior flux in inversions. Therefore, we compare the mismatches in
 366 OCO-2 and GOSAT inversions. The results are grouped global land and into the 11 TRANSCOM
 367 land regions, as shown in Table 3. The global land mean difference between modeled XCO₂ and the
 368 OCO-2 and GOSAT retrievals are 0.22 and 0.79 ppm, respectively, indicating that the GOSAT re-
 369 trieval would have stronger constraint on the prior fluxes. In most TRANSCOM regions except
 370 North Africa, the mismatches in GOSAT inversion are positive and larger than those of OCO-2 in-
 371 version. In Tropic Asia and South America Tropic, the sizable negative mismatches in OCO-2 in-
 372 version could account for a weak inverted carbon sink and an inverted carbon source in these two

373 regions, while in North Africa, the negative mismatch in GOSAT inversion may explain why a ra-
 374 ther weak sink is inverted for this region. The difference of mismatch between OCO-2 and GO-
 375 SAT inversions exhibits rather large spread, ranging from 0.16 to 1.33 pm, indicating the biases of
 376 two satellite XCO₂ retrievals differ greatly.

377 **Table 4.** Statistics of the OCO-2 and GOSAT retrievals uncertainties against the TCCON retrievals

	OCO-2			GOSAT		
	Bias/ppm	Stdev/ppm	N. of Obs.	Bias/ppm	Stdev/ppm	N. of Obs.
Bial	0.91	1.47	21	0.06	1.35	29
Darw	0.75	0.85	43	-0.41	1.62	44
Garm	-0.1	2.97	14	0.73	2.02	35
Lamo	0.04	1.09	56	-0.91	1.39	82
Laud	0.59	1.38	18	-0.79	1.7	30
Orle	1.49	1.18	24	-0.51	1.38	39
Park	0.5	1.26	29	-0.58	1.52	38
Soda	1.91	1.89	7	-0.54	2.58	9
Tsuk	0.93	1.95	16	-0.47	1.11	38
Woll	0.34	1.07	27	-0.36	1.56	45
All	0.6	1.45	255	-0.42	1.59	389

378

379 Moreover, the uncertainties of OCO-2 and GOSAT retrievals may be another reason for the dif-
 380 ferent performances in these two inversion experiments. We use TCCON retrievals to evaluate the
 381 uncertainties of OCO-2 and GOSAT XCO₂ retrievals. For satellite retrievals falling in the model
 382 grid box where TCCON sites are located, the closest TCCON retrievals in time or within two hours
 383 of satellite overpass time are chosen for comparison. We follow the procedures in Appendix A of
 384 Wunch et al. (2011) to do both prior profile and averaging kernel corrections. Table 4 shows the bi-
 385 ases and standard deviations grouped globally and at 10 TCCON sites where both OCO-2 and GO-
 386 SAT retrievals are available for comparison. The locations of these 10 sites are shown in Figure 2.
 387 Overall, GOSAT retrievals (-0.46 ppm) have lower bias than OCO-2 retrievals (0.6 ppm). At most

388 sites except Garm, OCO-2 retrievals have positive biases, while GOSAT retrievals tend to have
389 negative bias except at Bial and Garm sites. It also could be found that the spread of GOSAT data
390 biases are small, falling in the range of -0.36 to 0.58 ppm at most sites, while the spread of OCO₂
391 data biases is relatively large, with biases greater than 0.7 ppm at more than half of sites, in the
392 range of 0.34 to 0.59 ppm at 3 sites.

393 **4.3 Evaluation for the inversion results**

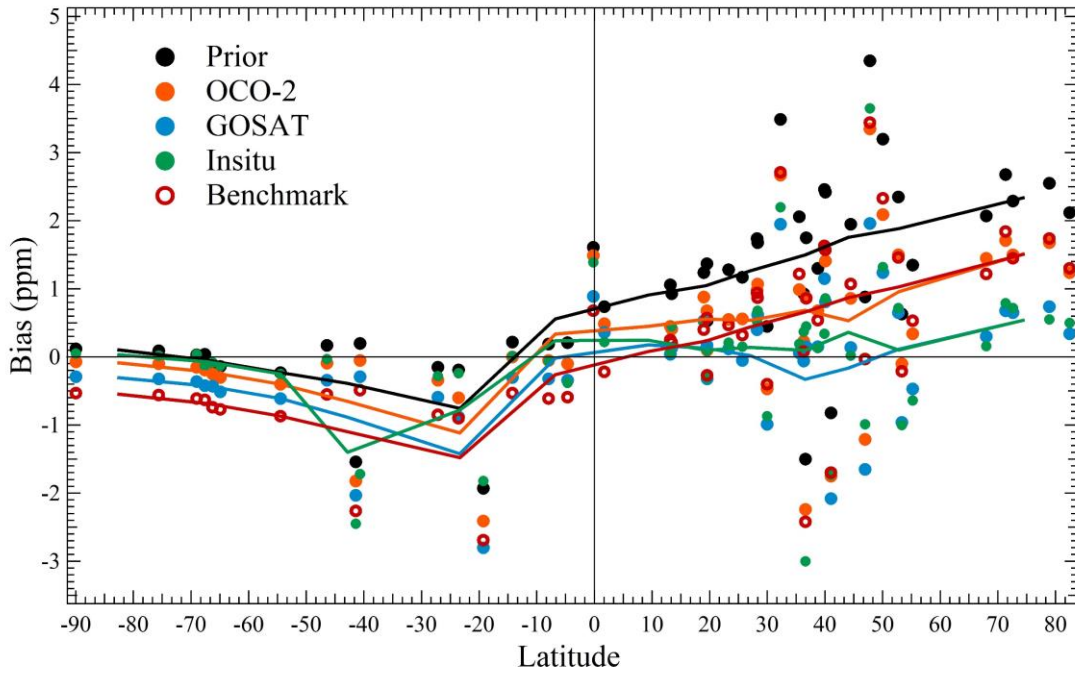
394 **4.3.1 Flask observations**

395 As shown in section 2.2, Flask observations from 52 sites are used to evaluate the inversion
396 results. Actually, there are much more flask observations in the dataset. When there are more than
397 one flask dataset for one site, we give priority to that from NOAA/ESL or that with more consistent
398 records. There are 56 sites with available flask observations for evaluation. In addition, during the
399 evaluations, we find that GEOS-Chem model is unable to capture the variations of CO₂ mixing ratios
400 at HPB, HUN, SGP and TAP sites, where the standard deviations of the deviations between the ob-
401 served and modeled mixing ratio are larger than 5 ppm. Therefore, we exclude these four sites and
402 use the rest 52 flask sites (shown in Figure 2) to evaluate the posterior mixing ratios. The GEOS-
403 Chem model is driven with the prior flux and the four posterior fluxes to obtain the prior and posterior
404 CO₂ mixing ratios. The simulated CO₂ mixing ratios are sampled at each observation site and within
405 half an hour of observation time.

406 Table 5 shows a summary of comparisons of the simulated CO₂ mixing ratios against the flask
407 measurements. The mean difference between the prior CO₂ mixing ratio and the flask measurements
408 is 0.93 ppm, with a standard deviation of 2.3 ppm. All four inversions show improvement in posterior
409 concentrations with reductions of biases. Not surprisingly, in situ inversion, using surface observa-
410 tions, shows the best improvement in posterior CO₂ mixing ratio with the largest reduction of bias
411 and standard deviation. GOSAT inversion achieve almost the same reductions of standard deviation
412 as in situ inversion. OCO-2 inversion gives larger bias and standard deviation than in situ and GOSAT

413 inversions. Benchmark inversion effectively reduces the bias but with little improvement in the re-
414 duction of standard deviations.

415 Figure 7 shows the biases at each observation site in different latitudes. It could be found that
416 the biases between the simulations and the observations in the northern hemisphere are significantly
417 larger than those in southern hemisphere since the carbon flux distribution of the northern hemisphere
418 is more complex than that of the southern hemisphere. When the prior flux is used, almost all sites in
419 the northern hemisphere have significant positive deviations, with an average of 1.7 ppm, while in
420 the southern hemisphere, the deviations are very small, with an average bias of only 0.08 ppm; when
421 using the posteriori flux from OCO-2 inversion, the deviations in most northern hemisphere sites are
422 slightly reduced, with an average deviation of 0.85 ppm, while in the southern hemisphere, at most
423 sites, the biases increase by variable amounts, with a mean of -0.13 ppm; when using the posterior
424 flux from GOSAT inversion, the deviations are significantly reduced to -0.04 ppm in the northern
425 hemisphere but further increased to -0.55 ppm in the southern hemisphere. In situ inversion shows
426 similar improvement in Northern Hemisphere as GOSAT inversion does, but also with litter improve-
427 ment in Southern Hemisphere. Though benchmark inversion effectively reduces the global bias, it
428 shows limited improvement in the reduction of biases at most sites. These suggest that GOSAT and
429 in situ inversions can effectively improve the carbon fluxes estimate in the northern hemisphere, but
430 overestimate the land sinks in the southern hemisphere, especially for GOSAT inversion.



431

432 **Figure 6.** Biases of the simulated CO₂ mixing ratios against the flask measurements in different lat-
 433 itudes (positive/negative biases represent modeled concentration being greater/less than the ob-
 434 served, the different color lines are the smooth of the corresponding marks)

435 4.3.2 TCCON observations

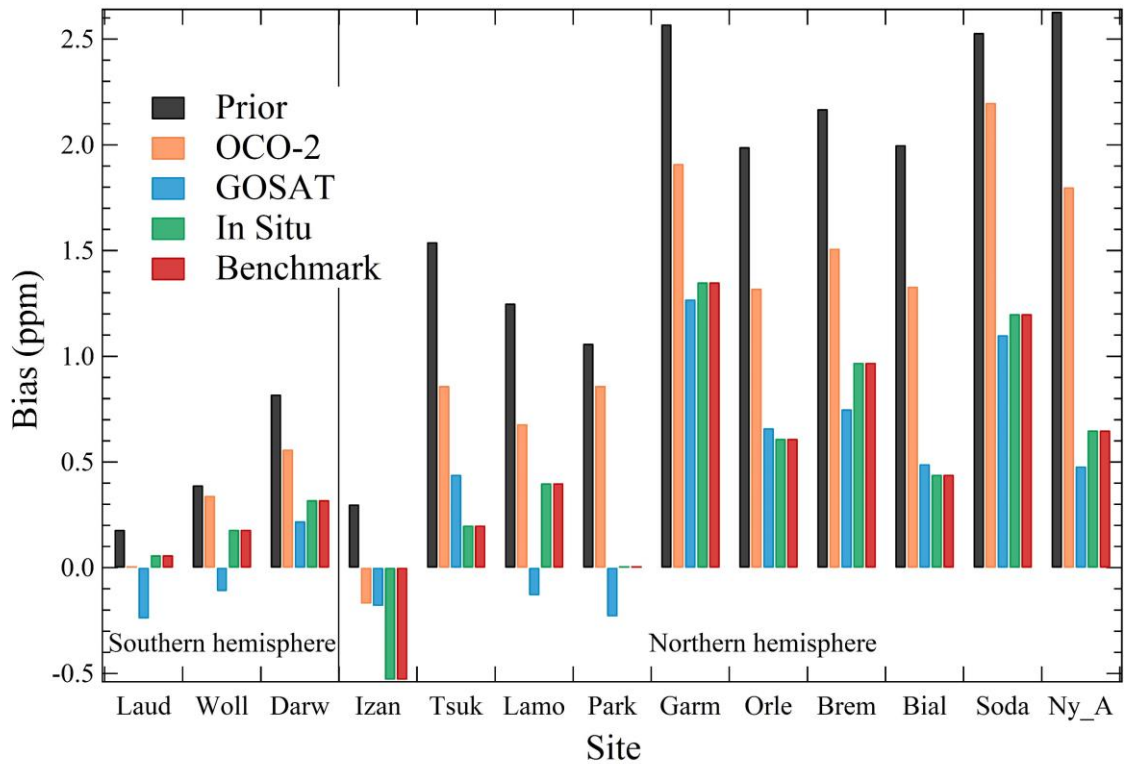
436 We also use ground XCO₂ observations from 13 TCCON sites (Figure 2) to evaluate our inver-
 437 sion results. The simulated CO₂ concentrations at 47 vertical levels are mapped into 71 TCCON
 438 levels. Following the approach of Wunch et al. (2011), using prior profiles and the averaging kernel
 439 from the TCCON dataset, we calculated the modeled XCO₂ values at 13 TCCON sites. Figure 6
 440 shows the comparison of modeled XCO₂ with TCCON observations. The mean difference between
 441 prior XCO₂ and TCCON retrievals is 1.16 ppm, with a standard deviation of 1.3 ppm. GOSAT in-
 442 version performs the best with the largest reductions of bias and standard deviations. Though OCO-
 443 2 inversion shows improvement in the reduction of standard deviation, it gives a relative large bias
 444 for posterior XCO₂. In situ inversion has the same reduction of standard deviation as GOSAT inver-
 445 sion. Benchmark inversion reduces the bias to 0.49 ppm and gives slight improvement in reducing
 446 standard deviation of posterior XCO₂.

447 Figure 7 shows the bias at each TCCON site. Obviously, the biases at all TCCON sites are pos-
448 itive when using the prior fluxes, ranging between 0.3 and 2.6 ppm. The biases at the sites in the
449 northern temperate and boreal areas are all above 1.5 ppm except for the Lamont site. For two of
450 the three TCCON sites in the southern hemisphere, the biases are changed to negative values when
451 using the posteriori fluxes from GOSAT data, further indicating the overestimation of carbon sinks
452 by GOSAT data in the southern hemisphere. In Northern Hemisphere, GOSAT, in situ and bench-
453 mark inversions significantly reduce the biases at most sites except Izan, Lamo and Park. However,
454 the biases at those sites remain relatively large. Since GOSAT and in situ inversions show evident
455 improvement at flask sites in Northern Hemisphere, the remaining large biases at TCCON sites may
456 not be due to the underestimate of Northern Land sink but the uncertainty of TCCON retrievals. At
457 Lamo and Park sites in North America, GOSAT inversion gives negative bias, suggesting it may
458 overestimate the carbon sink for North America Temperate. At Izan, the biases of posterior concen-
459 trations are up to -0.5 ppm from in situ and benchmark inversions, indicating the overestimate of
460 the carbon sink in North Africa by two inversions. For two of the three TCCON sites in the south-
461 ern hemisphere, the biases are changed to negative values when using the posteriori fluxes from
462 GOSAT data, further indicating the overestimation of carbon sinks by GOSAT data in the southern
463 hemisphere.

464 **Table 5.** Statistics of the model-data mismatch errors at the 52 surface flask sites and the 13 TCCON
465 sites

	Flask		TCCON	
	Bias	Stdev	Bias	Stdev
Prior	0.93	2.3	1.16	1.3
OCO-2	0.33	2.15	0.8	1.08
GOSAT	-0.19	2.05	0.22	1.04
In situ	-0.03	2.04	0.38	1.04
Benchmark	0.14	2.28	0.49	1.25

466



467

468 **Figure 7.** The biases between the modeled and observed XCO₂ at the 13 TCCON sites

469

470 5. Summary and Conclusions

471 In this study, we use both GOSAT and OCO-2 XCO₂ retrievals to constrain terrestrial ecosys-
 472 tem carbon fluxes from Oct 1, 2014 to Dec 31, 2015, using the GEOS-Chem 4D-Var data assimilation
 473 system. In addition, one inversion using in situ measurements and another inversion as a benchmark,
 474 are also conducted. The posterior carbon fluxes estimated from these four inversions at both global
 475 and regional scales during Jan 1 to Dec 31, 2015 are shown and discussed. We evaluate the posterior
 476 carbon fluxes by comparing the posterior CO₂ mixing ratios against observations from 52 surface
 477 flask sites and 13 TCCON sites.

478 Globally, the terrestrial ecosystem carbon sink (excluding biomass burning emissions) esti-
 479 mated from GOSAT data is stronger than that inferred from OCO-2 data and weaker than that from
 480 in situ inversion, but closest to the benchmark inversion estimate. Regionally, in most regions, the
 481 land sinks inferred from GOSAT data are also stronger than those from OCO-2 data. Compared with

482 the in situ inversion, GOSAT inversions have weaker sinks in Boreal and most Tropical lands, and
483 much stronger ones in Temperate lands. Compared with the prior fluxes, the inferred land sinks are
484 largely increased in the temperate regions, and decreased in tropical regions. There are largest changes
485 of the prior fluxes in Northern Temperate regions, followed by Tropical and Southern Temperate
486 regions, and the weakest in boreal regions. The different impact of XCO₂ on the carbon fluxes in
487 different regions is mainly related to the spatial coverage and the amount of XCO₂ data. Generally, a
488 larger amount of XCO₂ data in a region is corresponding to a larger change in the inverted carbon
489 flux in the same region.

490 Evaluations of the inversions using CO₂ concentrations from flask and TCCON measurements
491 showed that both posterior carbon fluxes estimated from OCO-2 and GOSAT retrievals could signif-
492 icantly improve the modeling of atmospheric CO₂ concentrations, and both the simulated surface CO₂
493 mixing ratio and XCO₂ concentrations with GOSAT posterior fluxes are much closer to the observa-
494 tions than those with OCO-2. Generally, in the northern hemisphere, the deviations are significantly
495 reduced, while in the southern hemisphere, the biases are slightly increased. Compared with in situ
496 and benchmark inversions, the GOSAT results are much closer to them in both comparisons with
497 flask and TCCON measurements. These suggest that GOSAT data can effectively improve the carbon
498 fluxes estimate in the northern hemisphere.

499 **Author contributions**

500 FJ and HW designed the research, HW conducted inverse modeling, HW and FJ conducted data anal-
501 ysis and wrote the paper, JW, WJ and JC participated in the discussion of the results and provided
502 input on the paper for revision before submission.

503 **Competing interests**

504 The authors declare that they have no conflict of interest.

505 **Acknowledgements**

506 This work is supported by the National Key R&D Program of China (Grant No: 2016YFA0600204), National
507 Natural Science Foundation of China (Grant No: 41571452), and the Fundamental Research Funds for the
508 Central Universities (Grant No: 090414380021). CarbonTracker CT2016 results provided by NOAA ESRL,
509 Boulder, Colorado, USA from the website at <http://carbontracker.noaa.gov>.

510

511 **References**

- 512 Andres, R. J., Gregg, J. S., Losey, L., Marland, G. and Boden, T. A.: Monthly, global emissions of carbon
513 dioxide from fossil fuel consumption. *Tellus B*, 63(3), 309–327, [https://doi.org/10.1111/j.1600-](https://doi.org/10.1111/j.1600-0889.2011.00530.x)
514 [0889.2011.00530.x](https://doi.org/10.1111/j.1600-0889.2011.00530.x), 2011.
- 515 Baker, D. F., Bösch, H., Doney, S. C., O’Brien, D., and Schimel, D. S.: Carbon source/sink information pro-
516 vided by column CO₂ measurements from the Orbiting Carbon Observatory, *Atmos. Chem. Phys.*, 10,
517 4145–4165, [https://doi.org/10.5194/acp-10-](https://doi.org/10.5194/acp-10-4145-2010) 4145-2010, 2010.
- 518 Basu, S., Guerlet, S., Butz, A., Houweling, S., Hasekamp, O., Aben, I., Krummel, P., Steele, P., Langenfelds,
519 R., Torn, M., Biraud, S., Stephens, B., Andrews, A., and Worthy, D.: Global CO₂ fluxes estimated from
520 GOSAT retrievals of total column CO₂, *Atmos. Chem. Phys.*, 13, 8695–8717,
521 [https://doi.org/10.5194/acp-](https://doi.org/10.5194/acp-13-8695-2013) 13-8695-2013, 2013.
- 522 Basu, S., Krol, M., Butz, A., Clerbaux, C., Sawa, Y., Machida, T., Matsueda, H., Frankenberg, C., Hasekamp,
523 O. P., and Aben, I.: The seasonal variation of the CO₂ flux over Tropical Asia estimated from GOSAT,
524 CONTRAIL, and IASI, *Geophys. Res. Lett.*, 41, 1809–1815, <https://doi.org/10.1002/2013GL059105>,
525 2014.
- 526 Blumenstock, T., Hase, F., Schneider, M., García, O.E., and Sepúlveda, E.: TCCON data from Izana, Tene-
527 rife, Spain, Release GGG2014R1. TCCON data archive, hosted by CaltechDATA, California Institute of
528 Technology, Pasadena, CA, U.S.A. <https://doi.org/10.14291/tccon.ggg2014.izana01.R1>, 2017.
- 529 Byrd, R. H., Nocedal, J. and Schnabel, R. B.: Representations of Quasi-Newton Matrices and their use in
530 Limited Memory Methods. *Math Program.* 63(4), 129–156. <https://doi.org/10.1007/BF01582063>, 1994.
- 531 CarbonTracker Team; (2017): Simulated observations of atmospheric carbon dioxide from CarbonTracker
532 release CT2016 (obspack_co2_1_CARBONTRACKER_CT2016_2017-02-06); NOAA Earth System Re-
533 search Laboratory, Global Monitoring Division. <http://dx.doi.org/10.15138/G3G599>"
- 534 Chatterjee, A., Gierach, M. M., Sutton, A. J., Feely, R. A., Crisp, D., Eldering, A., Gunson, M. R., O’Dell, C.
535 W., Stephens, B. B., and Schimel, D. S.: Influence of El Niño on atmospheric CO₂ over the tropical Pa-
536 cific Ocean: Findings from NASA’s OCO-2 mission, *Science*, 358, eaam5776,
537 <https://doi.org/10.1126/science.aam5776>, 2017.
- 538 Chevallier, F., Breon, F.-M., and Rayner, P. J.: Contribution of the Orbiting Carbon Observatory to the esti-
539 mation of CO₂ sources and sinks: Theoretical study in a variational data assimilation framework, *J. Ge-*
540 *ophys. Res.-Atmos.*, 112, d09307, <https://doi.org/10.1029/2006JD007375>, 2007.
- 541 Chevallier, F., Feng, L., Bösch, H., Palmer, P. I., and Rayner, P. J.: On the impact of transport model errors
542 for the estimation of CO₂ surface fluxes from GOSAT observations, *Geophys. Res. Lett.*, 37, L21803,
543 <https://doi.org/10.1029/2010GL044652>, 2010.
- 544 Chevallier, F., Palmer, P. I., Feng, L., Boesch, H., O’Dell, C. W., and Bousquet, P.: Toward robust and con-
545 sistent regional CO₂ flux estimates from in situ and spaceborne measurements of atmospheric CO₂, *Ge-*
546 *ophys. Res. Lett.*, 41, 1065–1070, <https://doi.org/10.1002/2013GL058772>, 2014.
- 547 Corbett, J. J., and Koehler, H. W.: Updated emissions from ocean shipping, *J. Geophys. Res.*, 108, 4650,
548 <https://doi.org/10.1029/2003JD003751>, D20, 2003.

- 549 Conway, T. J., Tans, P. P., Waterman, L. S., Thoning, K. W., Kitzis, D. R., Masarie, K. A., and Zhang, N.: Ev-
550 idence for interannual variability of the carbon cycle from the National Oceanic and Atmospheric Admin-
551 istration/Climate Monitoring and Diagnostics Laboratory Global Air Sampling Network, *J. Geophys.*
552 *Res.*, 99, 22831–22855, <https://doi.org/10.1029/94JD01951>, 1994.
- 553 Crisp, D., Pollock, H. R., Rosenberg, R., Chapsky, L., Lee, R. A. M., Oyafuso, F. A., Frankenberg, C.,
554 O’Dell, C. W., Bruegge, C. J., Doran, G. B., Eldering, A., Fisher, B. M., Fu, D., Gunson, M. R., Man-
555 drake, L., Osterman, G. B., Schwandner, F. M., Sun, K., Taylor, T. E., Wennberg, P. O., and Wunch, D.:
556 The on-orbit performance of the Orbiting Carbon Observatory-2 (OCO-2) instrument and its radiometri-
557 cally calibrated products, *Atmos. Meas. Tech.*, 10, 59–81, <https://doi.org/10.5194/amt-10-59-2017>, 2017.
- 558 Deng, F. and Chen, J. M.: Recent global CO₂ flux inferred from atmospheric CO₂ observations and its re-
559 gional analyses, *Biogeo- sciences*, 8, 3263–3281, <https://doi.org/10.5194/bg-8-3263-2011>, 2011.
- 560 Deng, F., Jones, D. B. A., Henze, D. K., Bousserez, N., Bowman, K. W., Fisher, J. B., Nassar, R., O’Dell, C.,
561 Wunch, D., Wennberg, P. O., Kort, E. A., Wofsy, S. C., Blumenstock, T., Deutscher, N. M., Griffith, D. W.
562 T., Hase, F., Heikkinen, P., Sherlock, V., Strong, K., Sussmann, R., and Warneke, T.: Inferring regional
563 sources and sinks of atmospheric CO₂ from GOSAT XCO₂ data, *Atmos. Chem. Phys.*, 14, 3703–3727,
564 <https://doi.org/10.5194/acp-14-3703-2014>, 2014.
- 565 Deng, F., Jones, D. B. A., O’Dell, C. W., Nassar, R., and Parazoo, N. C.: Combining GOSAT XCO₂ observa-
566 tions over land and ocean to improve regional CO₂ flux estimates, *J. Geophys. Res. Atmos.*, 121, 1896–
567 1913, <https://doi.org/10.1002/2015JD024157>, 2016.
- 568 Deutscher, N., Notholt, J., Messerschmidt, J., Weinzierl, C., Warneke, T., Petri, C., Grupe, P., and Katrynski,
569 K.: TCCON data from Bialystok, Poland, Release GGG2014R1. TCCON data archive, hosted by Cal-
570 techDATA, California Institute of Technology, Pasadena, CA, U.S.A.
571 <http://doi.org/10.14291/tcccon.ggg2014.bialystok01.R1/1183984>, 2017.
- 572 Eldering, A., Boland, S., Solish, B., Crisp, D., Kahn, P., and Gunson, M.: High precision atmospheric CO₂
573 measurements from space: The design and implementation of OCO-2, in: 2012 IEEE Aerospace Confer-
574 ence, 1–10, <https://doi.org/10.1109/AERO.2012.6187176>, 2012.
- 575 Eldering, A., O’Dell, C. W., Wennberg, P. O., Crisp, D., Gunson, M. R., Viatte, C., Avis, C., Braverman, A.,
576 Castano, R., Chang, A., Chapsky, L., Cheng, C., Connor, B., Dang, L., Doran, G., Fisher, B., Frankenberg,
577 C., Fu, D., Granat, R., Hobbs, J., Lee, R. A. M., Mandrake, L., McDuffie, J., Miller, C. E., Myers, V., Natraj,
578 V., O’Brien, D., Osterman, G. B., Oyafuso, F., Payne, V. H., Pol- lock, H. R., Polonsky, I., Roehl, C. M.,
579 Rosenberg, R., Schwand- ner, F., Smyth, M., Tang, V., Taylor, T. E., To, C., Wunch, D., and Yoshimizu, J.:
580 The Orbiting Carbon Observatory-2: first 18 months of science data products, *Atmos. Meas. Tech.*, 10,
581 549–563, <https://doi.org/10.5194/amt-10-549-2017>, 2017a.
- 582 Eldering, A., Wennberg, P. O., Crisp, D., Schimel, D. S., Gun- son, M. R., Chatterjee, A., Liu, J., Schwand-
583 ner, F. M., Sun, Y., O’Dell, C. W., Frankenberg, C., Taylor, T., Fisher, B., Oster- man, G. B., Wunch, D.,
584 Hakkarainen, J., Tamminen, J., and Weir, B.: The Orbiting Carbon Observatory-2 early science investiga-
585 tions of regional carbon dioxide fluxes, *Science*, 358, eaam5745, <https://doi.org/10.1126/sci->
586 [ence.aam5745](https://doi.org/10.1126/science.aam5745), 2017b.
- 587 Endresen, Ø., Sørgård, E., Behrens, H. L., Brett, P. O., and Isaksen, I. S. A.: A historical reconstruction of
588 ships’ fuel consumption and emissions, *J. Geophys. Res.*, 112, D12301,
589 <https://doi.org/10.1029/2006JD007630>, 2007.
- 590 Feng, L., Palmer, P. I., Parker, R. J., Deutscher, N. M., Feist, D. G., Kivi, R., Morino, I., and Sussmann, R.:
591 Estimates of European uptake of CO₂ inferred from GOSAT XCO₂ retrievals: Sensitivity to measurement
592 bias inside and outside Europe. *Atmos. Chem. Phys.*, 16, 1289–1302, <https://doi.org/10.5194/acp-16->
593 [1289-2016](https://doi.org/10.5194/acp-16-1289-2016), 2016.
- 594 Giglio, L., Randerson, J. T., and van der Werf, G. R.: Analysis of daily, monthly, and annual burned area us-
595 ing the fourth-generation global fire emissions database (GFED4) *J. Geophys. Res. Biogeosci.*, 118, 317–
596 328, <https://doi.org/10.1002/jgrg.20042>, 2013.

597 Griffith, D. W. T., Deutscher, N., Velazco, V. A., Wennberg, P. O., Yavin, Y., Keppel Aleks, G.,
598 Washenfelder, R., Toon, G. C., Blavier, J.-F., Murphy, C., Jones, N., Kettlewell, G., Connor,
599 B., Macatangay, R., Roehl, C., Ryzcek, M., Glowacki, J., Culgan, T., and Bryant, G.: TCCON
600 data from Darwin, Australia, Release GGG2014R0. TCCON data archive, hosted by Cal-
601 techDATA, California Institute of Technology, Pasadena, CA, U.S.A.
602 <http://doi.org/10.14291/tccon.ggg2014.darwin01.R0/1149290>, 2017a.

603 Griffith, D. W. T., Velazco, V. A., Deutscher, N., Murphy, C., Jones, N., Wilson, S., Macatangay,
604 R., Kettlewell, G., Buchholz, R. R., and Riggensbach, M.: TCCON data from Wollongong,
605 Australia, Release GGG2014R0. TCCON data archive, hosted by CaltechDATA, California
606 Institute of Technology, Pasadena, CA, U.S.A. <https://doi.org/10.14291/tccon.ggg2014.wol->
607 [longong01.R0/1149291](https://doi.org/10.14291/tccon.ggg2014.wol-longong01.R0/1149291), 2017b.

608 Gurney, K. R., Law, R. M., Denning, A. S., Rayner, P. J., Baker, D., Bousquet, P., Bruhwiler, L., Chen, Y.-H.,
609 Ciais, P., Fan, S., Fung, I. Y., Gloor, M., Heimann, M., Higuchi, K., John, J., Maki, T., Maksyutov, S.,
610 Masarie, K., Peylin, P., Prather, M., Pak, B. C., Randerson, J., Sarmiento, J., Taguchi, S., Takahashi, T.,
611 and Yuen, C.-W.: Towards robust regional estimates of CO₂ sources and sinks using atmospheric
612 transport models, *Nature*, 415, 626–630, 2002.

613 Henze, D. K., Hakami, A. and Seinfeld, J. H.: Development of the adjoint of GEOS-Chem, *Atmos. Chem.*
614 *Phys.*, 7, 2413-2433, 2007.

615 Heymann, J., Reuter, M., Buchwitz, M., Schneising, O., Bovensmann, H., Burrows, J. P., Massart, S., Kai-
616 ser, J. W., and Crisp, D.: CO₂ emission of Indonesian fires in 2015 estimated from satellite-derived atmos-
617 pheric CO₂ concentrations, *Geophys. Res. Lett.*, 44, 1537–1544, <https://doi.org/10.1002/2016GL072042>,
618 2017.

619 Houweling, S., Breon, F.-M., Aben, I., Rödenbeck, C., Gloor, M., Heimann, M., and Ciais, P.: Inverse mod-
620 eling of CO₂ sources and sinks using satellite data: a synthetic inter-comparison of measurement tech-
621 niques and their performance as a function of space and time, *Atmos. Chem. Phys.*, 4, 523–538,
622 <https://doi.org/10.5194/acp-4-523-2004>, 2004.

623 Houweling, S., Aben, I., Breon, F.-M., Chevallier, F., Deutscher, N., Engelen, R., Gerbig, C., Griffith, D.,
624 Hungershoefer, K., Macatangay, R., Marshall, J., Notholt, J., Peters, W., and Serrar, S.: The importance of
625 transport model uncertainties for the estimation of CO₂ sources and sinks using satellite measurements,
626 *Atmos. Chem. Phys.*, 10, 9981–9992, <https://doi.org/10.5194/acp-10-9981-2010>, 2010.
627

628 Houweling, S., Baker, D., Basu, S., Boesch, H., Butz, A., Chevallier, F., Deng, F., Dlugokencky, E. J., Feng,
629 L., Ganshin, A., Hasekamp, O., Jones, D., Maksyutov, S., Marshall, J., Oda, T., O’Dell, C. W.,
630 Oshchepkov, S., Palmer, P. I., Peylin, P., Poussi, Z., Reum, F., Takagi, H., Yoshida, Y., and Zhuravlev, R.:
631 An intercomparison of inverse models for estimating sources and sinks of CO₂ using GOSAT measure-
632 ments, *J. Geophys. Res.-Atmos.*, 120, 5253–5266, <https://doi.org/10.1002/2014JD022962>, 2015.

633 Hungershoefer, K., Breon, F.-M., Peylin, P., Chevallier, F., Rayner, P., Klonecki, A., Houweling, S., and Mar-
634 shall, J.: Evaluation of various observing systems for the global monitoring of CO₂ surface fluxes, *Atmos.*
635 *Chem. Phys.*, 10, 10503–10520, <https://doi.org/10.5194/acp-10-10503-2010>, 2010.

636 Jiang, Z., Jones, D. B. A., Kopacz, M., Liu, J., Henze, D. K., and Heald, C.: Quantifying the impact of model
637 errors on top-down estimates of carbon monoxide emissions using satellite observations, *J. Geophys.*
638 *Res.*, 116, D15306, <https://doi.org/10.1029/2010JD015282>, 2011.

639 Kim, B. Y., Fleming, G. G., Lee, J. J., Waitz, I. A., Clarke, J.-P., Balasubramanian, S., Malwitz, A., Klima,
640 K., Locke, M., Holsclaw, C. A., Maurice, L. Q., Gupta, M. L.: System for assessing Aviation’s Global
641 Emissions (SAGE), Part 1: Model description and inventory results, *Transportation Research Part D:*
642 *Transport and Environment*, 12(5), 325-346, <https://doi.org/10.1016/j.trd.2007.03.007>, 2007.

643 Kim, J., Kim, H. M., Cho, C.-H., Boo, K.-O., Jacobson, A. R., Sasakawa, M., Machida, T., Arshinov, M., and
644 Fedoseev, N.: Impact of Siberian observations on the optimization of surface CO₂ flux, *Atmos. Chem.*
645 *Phys.*, 17, 2881-2899, <https://doi.org/10.5194/acp-17-2881-2017>, 2017.

- 646 Kivi, R., Heikkinen, P., and Kyro, E.: TCCON data from Sodankyla, Finland, Release
647 GGG2014R0. TCCON data archive, hosted by CaltechDATA, California Institute of Technol-
648 ogy, Pasadena, CA, U.S.A. <https://doi.org/10.14291/tccon.ggg2014.sodankyla01.R0/1149280>,
649 2017.
- 650 Kopacz, M., Jacob, D. J., Henze, D. K., Heald, C. L., Streets, D. G., and Zhang, Q.: A comparison of analyti-
651 cal and adjoint Bayesian inversion methods for constraining Asian sources of CO using satellite
652 (MOPITT) measurements of CO columns, *J. Geophys. Res.*, 114, D04305,
653 <https://doi.org/10.1029/2007JD009264>, 2009.
- 654 Kopacz, M., Jacob, D. J., Fisher, J. A., Logan, J. A., Zhang, L., Megretskaia, I. A., Yantosca, R. M., Singh, K.,
655 Henze, D. K., Burrows, J. P., Buchwitz, M., Khlystova, I., McMillan, W. W., Gille, J. C., Edwards, D. P.,
656 Eldering, A., Thouret, V., and Nedelec, P.: Global estimates of CO sources with high resolution by adjoint
657 inversion of multiple satellite datasets (MOPITT, AIRS, SCIAMACHY, TES), *Atoms. Chem. Phys.*, 10,
658 855-876, 2010.
- 659 Kuze, A., Suto, H., Nakajima, M., and Hamazaki, T.: Thermal and near infrared sensor for carbon observa-
660 tion Fourier-transform spectrometer on the Greenhouse Gases Observing Satellite for greenhouse gases
661 monitoring. *Appl. Opt.*, 48, 6716, <https://doi.org/10.1364/AO.48.006716>, 2009.
- 662 Le Quéré, C., Andrew, R. M., Friedlingstein, P., Sitch, S., Pongratz, J., Manning, A. C., Korsbakken, J. I.,
663 Peters, G. P., Canadell, J. G., Jackson, R. B., Boden, T. A., Tans, P. P., Andrews, O. D., Arora, V. K., Bak-
664 ker, D. C. E., Barbero, L., Becker, M., Betts, R. A., Bopp, L., Chevallier, F., Chini, L. P., Ciais, P., Cosca,
665 C. E., Cross, J., Currie, K., Gasser, T., Harris, I., Hauck, J., Haverd, V., Houghton, R. A., Hunt, C. W.,
666 Hurtt, G., Ilyina, T., Jain, A. K., Kato, E., Kautz, M., Keeling, R. F., Klein Goldewijk, K., Körtzinger, A.,
667 Landschützer, P., Lefèvre, N., Lenton, A., Lienert, S., Lima, I., Lombardozi, D., Metzl, N., Millero, F.,
668 Monteiro, P. M. S., Munro, D. R., Nabel, J. E. M. S., Nakaoka, S.-I., Nojiri, Y., Padin, X. A., Pregon, A.,
669 Pfeil, B., Pierrot, D., Poulter, B., Rehder, G., Reimer, J., Rödenbeck, C., Schwinger, J., Séférian, R.,
670 Skjelvan, I., Stocker, B. D., Tian, H., Tilbrook, B., Tubiello, F. N., van der Laan-Luijkx, I. T., van der
671 Werf, G. R., van Heuven, S., Viovy, N., Vuichard, N., Walker, A. P., Watson, A. J., Wiltshire, A. J.,
672 Zaehle, S., and Zhu, D.: Global Carbon Budget 2017, *Earth Syst. Sci. Data*, 10, 405-448,
673 <https://doi.org/10.5194/essd-10-405-2018>, 2018.
- 674 Liu, J., Bowman, K. W., Lee, M., Henze, D. K., Bousserez, N., Brix, H., Collatz, G. J., Menemenlis, D., Ott,
675 L., Pawson, S., Jones, D., and Nassar, R.: Carbon monitoring system flux estimation and attribution: im-
676 pact of ACOS-GOSAT XCO₂ sampling on the inference of terrestrial biospheric sources and sinks, *Tellus*
677 *B*, 66, 22486, <https://doi.org/10.3402/tellusb.v66.22486>, 2014.
- 678 Liu, J., Bowman, K. W., Schimel, D. S., Parazoo, N. C., Jiang, Z., Lee, M., Bloom, A. A., Wunch, D., Frank-
679 enberg, C., Sun, Y., O'Dell, C. W., Gurney, K. R., Menemenlis, D., Gierach, M., Crisp, D., and Eldering,
680 A.: Contrasting carbon cycle responses of the tropical continents to the 2015–2016 El Niño, *Science*, 358,
681 eaam5690, <https://doi.org/10.1126/science.aam5690>, 2017.
- 682 Maksyutov, S., Takagi, H., Valsala, V. K., Saito, M., Oda, T., Saeki, T., Belikov, D. A., Saito, R., Ito, A., Yo-
683 shida, Y., Morino, I., Uchino, O., Andres, R. J., and Yokota, T.: Regional CO₂ flux estimates for 2009–
684 2010 based on GOSAT and ground- based CO₂ observations, *Atmos. Chem. Phys.*, 13, 9351–9373,
685 <https://doi.org/10.5194/acp-13-9351-2013>, 2013.
- 686 Miller, C. E., Crisp, D., DeCola, P. L., Olsen, S. C., Randerson, J. T., Michalak, A. M., Alkhaled, A., Rayner,
687 P., Jacob, D. J., Suntharalingam, P., Jones, D. B. A., Denning, A. S., Nicholls, M. E., Doney, S. C., Paw-
688 son, S., Boesch, H., Connor, B. J., Fung, I. Y., O'Brien, D., Salawitch, R. J., Sander, S. P., Sen, B., Tans,
689 P., Toon, G. C., Wennberg, P. O., Wofsy, S. C., Yung, Y. L., and Law, R. M.: Precision requirements for
690 space-based XCO₂ data, *J. Geophys. Res.*, 112, D10314, <https://doi.org/10.1029/2006JD007659>, 2007.
- 691 Miller, S. M., Michalak, A. M., Yadav, V., and Tadić, J. M.: Characterizing biospheric carbon balance using
692 CO₂ observations from the OCO-2 satellite, *Atmos. Chem. Phys.*, 18, 6785-6799,
693 <https://doi.org/10.5194/acp-18-6785-2018>, 2018.
- 694 Morino, I., Matsuzaki, T., and Shishime, A.: TCCON data from Tsukuba, Ibaraki, Japan, 125HR,
695 Release GGG2014R2. TCCON data archive, hosted by CaltechDATA, California Institute of

696 Technology, Pasadena, CA, U.S.A. <http://doi.org/10.14291/tccon.ggg2014.tsukuba02.R2>,
697 2017.

698 Nassar, R., Jones, D. B. A., Suntharalingam, P., Chen, J. M., Andres, R. J., Wecht, K. J., Yantosca, R. M., Ku-
699 lawik, S. S., Bowman, K. W., Worden, J. R., Machida, T., and Matsueda, H.: Modeling global atmos-
700 pheric CO₂ with improved emission inventories and CO₂ production from the oxidation of other carbon
701 species, *Geosci. Model Dev.*, 3, 689–716, <https://doi.org/10.5194/gmd-3-689-2010>, 2010.

702 Nassar, R., Hill, T. G., McLinden, C. A., Wunch, D., Jones, D. B. A., and Crisp, D.: Quantifying CO₂ emis-
703 sions From Individual Power Plants from Space, *Geophys. Res. Lett.*, 44, 10045– 10053,
704 <https://doi.org/10.1002/2017GL074702>, 2017.

705 Notholt, J., Petri, C., Warneke, T., Deutscher, N., Buschmann, M., Weinzierl, C., Macatangay,
706 R., and Grupe, P.: TCCON data from Bremen, Germany, Release GGG2014R0. TCCON data
707 archive, hosted by CaltechDATA, California Institute of Technology, Pasadena, CA, U.S.A.
708 <https://doi.org/10.14291/tccon.ggg2014.bremen01.R0/1149275>, 2017a.

709 Notholt, J., Schrems, O., Warneke, T., Deutscher, N., Weinzierl, C., Palm, M., Buschmann, M.,
710 and AWI-PEV Station Engineers: TCCON data from Ny Alesund, Spitzbergen, Norway, Re-
711 lease GGG2014R0. TCCON data archive, hosted by CaltechDATA, California Institute of
712 Technology, Pasadena, CA, U.S.A. <https://doi.org/10.14291/tccon.ggg2014.nyale->
713 [sund01.R0/1149278](https://doi.org/10.14291/tccon.ggg2014.nyalesund01.R0/1149278), 2017b.

714 ObsPack: Cooperative Global Atmospheric Data Integration Project, Multi-laboratory compilation of atmospheric
715 carbon dioxide data for the period 1957–2015, *obspack_co2_1_GLOBALVIEWplus_v2.1_2016-09-02*,
716 NOAA Earth System Research Laboratory, Global Monitoring Division, <https://doi.org/10.15138/G3059Z>,
717 2016.

718 O'Dell, C., Connor, B., Bösch, H., O'Brien, D., Frankenberg, C., Castano, R., Christi, M., Eldering, D.,
719 Fisher, B., Gunson, M., McDuffie, J., Miller, C. E., Natraj, V., Oyafuso, F., Polonsky, I., Smyth, M., Tay-
720 lor, T., Toon, G., Wennberg, P., and Wunch, D.: The ACOS CO₂ retrieval algorithm – Part 1: Description
721 and validation against synthetic observations, *Atmos. Meas. Tech.*, 5, 99-121, <https://doi.org/10.5194/amt->
722 [5-99-2012](https://doi.org/10.5194/amt-5-99-2012), 2012.

723 Oda, T. and Maksyutov, S. 2011. A very high-resolution (1 km x 1 km) global fossil fuel CO₂ emission in-
724 ventory derived using a point source database and satellite observations of nighttime lights. *Atmos. Chem.*
725 *Phys.* **11**, 543 – 556.

726 Park, B. C. and Prather, M. J.: CO₂ source inversions using satellite observations of the upper troposphere,
727 *Geophys. Res. Lett.*, 28, 4571–4574, <https://doi.org/10.1029/2001GL013604>, 2001.

728 Parrington, M., Palmer, P. I., Henze, D. K., Tarasick, D. W., Hyer, E. J., Owen, R. C., Clerbaux, C., Bowman,
729 K. W., Deeter, M. N., Barratt, E. M., Coheur, P.-F., Hurtmans, D., George, M., and Worden, J. R.: The in-
730 fluence of boreal biomass burning emissions on the distribution of tropospheric ozone over North Amer-
731 ica and the North Atlantic during 2010, *Atmos. Chem. Phys.*, 12, 2077-2098, 2012.

732 Patra, P. K., Crisp, D., Kaiser, J. W., Wunch, D., Saeki, T., Ichii, K., Sekiya, T., Wennberg, P. O., Feist, D. G.,
733 Pollard, D. F., Griffith, D. W. T., Velazco, V. A., De Maziere, M., Sha, M. K., Roehl, C., Chatterjee, A.,
734 and Ishijima, K.: The Orbiting Carbon Observa- tory (OCO-2) tracks 2–3 peta-gram increase in carbon
735 release to the atmosphere during the 2014–2016 El Niño, *Sci. Rep.-UK*, 7, 13567,
736 <https://doi.org/10.1038/s41598-017-13459-0>, 2017.

737 Peters, W., Jacobson, A. R., Sweeney, C., Andrews, A. E., Conway, T. J., Masarie, K., Miller, J. B., Bruh-
738 wiler, L. M. P., P'etron, G., Hirsch, A. I., Worthy, D. E. J., Werf, G. R. V. D., Randerson, J. T., Wennberg,
739 P. O., Krol, M. C., and Tans, P. P.: An atmospheric perspective on North American carbon dioxide ex-
740 change: CarbonTracker, *P. Natl. Acad. Sci.*, 104, 18925–18930, 2007..

741 Peylin, P., Law, R. M., Gurney, K. R., Chevallier, F., Jacobson, A. R., Maki, T., Niwa, Y., Patra, P. K., Peters,
742 W., Rayner, P. J., Rödenbeck, C., van der Laan-Luijkx, I. T., and Zhang, X.: Global atmospheric carbon
743 budget: results from an ensemble of atmospheric CO₂ inversions, *Biogeosciences*, 10, 6699–6720,
744 <https://doi.org/10.5194/bg-10-6699-2013>, 2013.

- 745 Potter, C. S., Randerson, J. T., Field, C. B., Matson, P. A., Vitousek, P. M., Mooney, H. A., and Klooster, S.
746 A.: Terrestrial ecosystem production: A process model based on global satellite and surface data, *Global*
747 *Biogeochem. Cycles*, 7(4), 811–841, <https://doi.org/10.1029/93GB02725>, 1993.
- 748 Rayner, P. J. and O'Brien, D. M.: The utility of remotely sensed CO₂ concentration data in surface source
749 inversions, *Geophys. Res. Lett.*, 28, 175–178, <https://doi.org/10.1029/2000GL011912>, 2001.
- 750 Reuter, M., Buchwitz, M., Hilker, M., Heymann, J., Schneising, O., Pillai, D., Bovensmann, H., Burrows, J.
751 P., Bösch, H., Parker, R., Butz, A., Hasekamp, O., O'Dell, C. W., Yoshida, Y., Gerbig, C., Nehrkorn, T.,
752 Deutscher, N. M., Warneke, T., Notholt, J., Hase, F., Kivi, R., Sussmann, R., Machida, T., Matsueda, H.,
753 and Sawa, Y.: Satellite-inferred European carbon sink larger than expected, *Atmos. Chem. Phys.*, 14,
754 13739–13753, <https://doi.org/10.5194/acp-14-13739-2014>, 2014.
- 755 Reuter, M., Buchwitz, M., Hilker, M., Heymann, J., Bovensmann, H., Burrows, J. P., Houweling, S., Liu, Y.
756 Y., Nassar, R., Chevallier, F., Ciais, P., Marshall, J., and Reichstein, M.: How Much CO₂ Is Taken Up by
757 the European Terrestrial Biosphere?. *Bull. Amer. Meteor. Soc.*, 98, 665–671,
758 <https://doi.org/10.1175/BAMS-D-15-00310.1>, 2017.
- 759 Rienecker, M. M., Suarez, M. J., Todling, R., Bacmeister, J., Takacs, L. and co-authors: The GEOS-5 Data
760 Assimilation System-Documentation of versions 5.0.1 and 5.1.0, and 5.2.0 NASA Tech. Rep. Series on
761 Global Modeling and Data Assimilation, NASA/TM-2008-104606, Vol. 27, 92 pp, 2008.
- 762 Rodgers, C. D.: *Inverse Methods for Atmospheric Sounding: Theory and Practice*, World Scientific Publish-
763 ing Co Inc, Singapore, chapter 2, 2000.
- 764 Saeki, T., Maksyutov, S., Saito, M., Valsala, V., Oda, T., Andres, R. J., Belikov, D., Tans, P., Dlugokencky,
765 E., Yoshida, Y., Morino, I., Uchino, O., and Yokota, T.: Inverse modeling of CO₂ fluxes using GOSAT
766 data and multi-year ground-based obser- vations, *SOLA*, 9, 45–50, <https://doi.org/10.2151/sola.2013-011>,
767 2013.
- 768 Sherlock, V., Connor, B., Robinson, J., Shiona, H., Smale, D., and Pollard, D.: TCCON data from
769 Lauder, New Zealand, 125HR, Release GGG2014R0. TCCON data archive, hosted by Cal-
770 techDATA, California Institute of Technology, Pasadena, CA, U.S.A.
771 <https://doi.org/10.14291/tcon.ggg2014.lauder02.R0/1149298>, 2017.
- 772 Singh, K., Jardak, M., Sandu, A., Bowman, K., Lee, M., and Jones, D.: Construction of non-diagonal back-
773 ground error covariance matrices for global chemical data assimilation, *Geosci. Model Dev.*, 4, 299–316,
774 <https://doi.org/10.5194/gmd-4-299-2011>, 2011.
- 775 Suntharalingam, P., Jacob, D. J., Palmer, P. I., Logan, J. A., Yantosca, R. M. and co-authors: Improved quan-
776 tification of Chinese carbon fluxes using CO₂/CO correlations in Asian outflow. *J. Geophys. Res.* 109,
777 D18S18, <https://doi.org/10.1029/2003JD004362>, 2004.
- 778 Sussmann, R., and Rettinger, M.: TCCON data from Garmisch, Germany, Release GGG2014R2.
779 TCCON data archive, hosted by CaltechDATA, California Institute of Technology, Pasadena,
780 CA, U.S.A. <https://doi.org/10.14291/tcon.ggg2014.garmisch01.R2>, 2017.
- 781 Takagi, H., Saeki, T., Oda, T., Saito, M., Valsala, V., Belikov, D., Saito, R., Yoshida, Y., Morino, I., Uchino,
782 O., Andres, R. J., Yokota, T., and Maksyutov, S.: On the benefit of GOSAT observations to the estimation
783 of regional CO₂ fluxes, *SOLA*, 7, 161–164, <https://doi.org/10.2151/sola.2011-041>, 2011.
- 784 Tarantola, A.: *Inverse Problem Theory and Methods for Model Parameter Estimation*, Soc. Industr. App.l
785 Math., Philadelphia, PA, USA, 2004.
- 786 van der Werf, G. R., Randerson, J. T., Giglio, L., Collatz, G. J., Mu, M., Kasibhatla, P. S., Morton, D. C., De-
787 Fries, R. S., Jin, Y., and van Leeuwen, T. T.: Global fire emissions and the contribution of deforestation,
788 savanna, forest, agricultural, and peat fires (1997–2009), *Atmos. Chem. Phys.*, 10, 11707–11735,
789 <https://doi.org/10.5194/acp-10-11707-2010>, 2010.
- 790 Wang, X., Guo, Z., Huang, Y. P., Fan, H. J., and Li, W. B.: A cloud detection scheme for the Chinese carbon
791 dioxide observation satellite (TANSAT). *Adv. Atmos. Sci.*, 34(1), 16–25, [https://doi.org/10.1007/s00376-](https://doi.org/10.1007/s00376-016-6033-y)
792 016-6033-y, 2017.

- 793 Warneke, T., Messerschmidt, J., Notholt, J., Weinzierl, C., Deutscher, N., Petri, C., Grupe, P.,
794 Vuillemin, C., Truong, F., Schmidt, M., Ramonet, M., and Parmentier, E.: TCCON data from
795 Orleans, France, Release GGG2014R0. TCCON data archive, hosted by CaltechDATA, Cali-
796 fornia Institute of Technology, Pasadena, CA, U.S.A.
797 <https://doi.org/10.14291/tcon.ggg2014.orleans01.R0/1149276>, 2017.
- 798 Wennberg, P. O., Roehl, C., Wunch, D., Toon, G. C., Blavier, J.-F., Washenfelder, R., Keppel-Aleks, G., Al-
799 len, N., and Ayers, J.: TCCON data from Park Falls, Wisconsin, USA, Release GGG2014R1. TCCON
800 data archive, hosted by CaltechDATA, California Institute of Technology, Pasadena, CA, U.S.A.
801 <http://doi.org/10.14291/tcon.ggg2014.parkfalls01.R1>, 2017.
- 802 Wennberg, P. O., Wunch, D., Roehl, C., Blavier, J.-F., Toon, G. C., Allen, N., Dowell, P., Teske, K., Martin,
803 C., and Martin, J.: TCCON data from Lamont, Oklahoma, USA, Release GGG2014R1. TCCON data ar-
804 chive, hosted by CaltechDATA, California Institute of Technology, Pasadena, CA, U.S.A.
805 <https://doi.org/10.14291/tcon.ggg2014.lamont01.R1/1255070>, 2017. Wilkerson, J. T., Jacobson, M. Z.,
806 Malwitz, A., Balasubramanian, S., Wayson, R., Fleming, G., Naiman, A. D., and Lele, S. K.: Analysis of
807 emission data from global commercial aviation: 2004 and 2006, *Atmos. Chem. Phys.*, 10, 6391-6408,
808 <https://doi.org/10.5194/acp-10-6391-2010>, 2010.
- 809 Wunch, D., Wennberg, P. O., Toon, G. C., Connor, B. J., Fisher, B., Osterman, G. B., Frankenberg, C., Man-
810 drake, L., O'Dell, C., Ahonen, P., Biraud, S. C., Castano, R., Cressie, N., Crisp, D., Deutscher, N. M.,
811 Eldering, A., Fisher, M. L., Griffith, D. W. T., Gunson, M., Heikkinen, P., Keppel-Aleks, G., Kyrö, E.,
812 Lindenmaier, R., Macatangay, R., Mendonca, J., Messerschmidt, J., Miller, C. E., Morino, I., Notholt, J.,
813 Oyafuso, F. A., Rettinger, M., Robinson, J., Roehl, C. M., Salawitch, R. J., Sherlock, V., Strong, K., Suss-
814 mann, R., Tanaka, T., Thomp- son, D. R., Uchino, O., Warneke, T., and Wofsy, S. C.: A method for evalu-
815 ating bias in global measurements of CO₂ total columns from space, *Atmos. Chem. Phys.*, 11, 12317–
816 12337, <https://doi.org/10.5194/acp-11-12317-2011>, 2011.
- 817 Wunch, D., Wennberg, P. O., Osterman, G., Fisher, B., Naylor, B., Roehl, C. M., O'Dell, C., Mandrake, L.,
818 Viatte, C., Kiel, M., Griffith, D. W. T., Deutscher, N. M., Velazco, V. A., Notholt, J., Warneke, T., Petri,
819 C., De Maziere, M., Sha, M. K., Sussmann, R., Rettinger, M., Pollard, D., Robinson, J., Morino, I.,
820 Uchino, O., Hase, F., Blumenstock, T., Feist, D. G., Arnold, S. G., Strong, K., Mendonca, J., Kivi, R.,
821 Heikkinen, P., Iraci, L., Podolske, J., Hillyard, P. W., Kawakami, S., Dubey, M. K., Parker, H. A., Sepul-
822 veda, E., García, O. E., Te, Y., Jeseck, P., Gunson, M. R., Crisp, D., and Eldering, A.: Comparisons of the
823 Orbiting Carbon Observatory-2 (OCO-2) XCO₂ measurements with TCCON, *At- mos. Meas. Tech.*, 10,
824 2209–2238, <https://doi.org/10.5194/amt-10-2209-2017>, 2017.
- 825 Yang, D. X., Liu, Y., Cai, Z. N., Chen, X., Yao, L., and Lu, D. R.: First global carbon dioxide maps produced
826 from TanSat measurements. *Adv. Atmos. Sci.*, 35(6), 621–623, [https://doi.org/10.1007/s00376-018-7312-](https://doi.org/10.1007/s00376-018-7312-6)
827 6, 2018.
- 828 Zhu, C., Byrd, R. H., Lu, P. and Nocedal, J.: L-BFGS-B: algorithm 778: L-BFGS-B, FORTRAN routines for
829 large scale bound constrained optimization. *ACM Trans. Math. Softw.* 23(4), 550_560.
830 <https://doi.org/10.1145/279232.279236>, 1997.

831

832